https://doi.org/10.5194/egusphere-2025-6002
Preprint. Discussion started: 17 December 2025

TREED (v1.0): a trait- and optimality-based eco-evolutionary vegetation model for the deep past and the present

Julian Rogger[1,2,3,4], Khushboo Gurung[5], Emanuel B. Kopp[6], William J. Matthaeus[7], Benjamin J. W. Mills[5], Benjamin D. Stocker[8,9], Taras V. Gerya[2], Loïc Pellissier[1,3]

[1]Department of Environmental Systems Science, ETH Zurich, Zurich, Switzerland
[2]Department of Earth and Planetary Sciences, ETH Zurich, Zurich, Switzerland
[3]Swiss Federal Institute for Forest, Snow and Landscape Research, Birmensdorf, Switzerland
[4]School of Geographical Sciences, University of Bristol, Bristol, United Kingdom
[5]School of Earth and Environment, University of Leeds, Leeds, Switzerland
[6]Department of Evolutionary Biology and Environmental Studies, University of Zurich, Zurich, Switzerland
[7]School of Natural Sciences, Trinity College, Dublin, Ireland
[8]Institute of Geography, University of Bern, Bern, Switzerland
[9]Oeschger Centre for Climate Change Research, University of Bern, Bern, Switzerland

Correspondence to: Julian Rogger (jul.rogger@gmail.com)

Abstract

We present the TREED model (TRait Ecology and Evolution over Deep time), a trait- and optimality-based vegetation model to simulate vegetation structure, carbon cycling and eco-evolutionary adaptation dynamics to climate and CO_2 changes across geologic time scales. The global grid-based vegetation model represents plant carbon allocation and trait evolution as a set of carbon economic trade-offs. Based on optimality principles, it is assumed that functional traits of the modelled community-representative average plants evolve towards an optimum that maximizes height growth while maintaining a positive carbon balance. The considered trait trade-offs resolve the potential plant height, leaf carbon pool size, leaf longevity, and phenology as the major axes of plant trait variation. Based on these key traits, whole-plant structure and functioning are derived using functional and allometric relationships. In its eco-evolutionary mode, vegetation-mediated carbon cycling can be tracked over the course of climatic transitions, testing the effects of the speed of evolutionary trait adaptation and dispersal dynamics. Moreover, with its generalized plant physiology, continuous trait space, and lack of pre-defined functional types, the model can be used to calculate metrics of biodiversity, including indices of the functional diversity and species richness potential. With a low computational demand, a flexible time stepping scheme and scalable adaptation parameters, TREED is intended to simulate biological and environmental transitions across time scales spanning from centuries to millions of years. Here, we present the underlying theory and model functions and evaluate model outputs against present-day observations. We show that the trait- and optimality-based approach captures major patterns in present-day vegetation-mediated carbon and water fluxes, biomass carbon storage, vegetation height, leaf traits, as well as the global distribution of plant biodiversity. Finally, we illustrate its application in the context of paleoclimate and palaeoecological research using the Paleocene-Eocene Thermal Maximum as a case study and show how eco-evolutionary adaptation dynamics of terrestrial ecosystems may strongly affect global carbon cycle dynamics during hyperthermal events. The TREED model is a step towards a more self-

https://doi.org/10.5194/egusphere-2025-6002
Preprint. Discussion started: 17 December 2025

consistent and parameter-scarce representation of vegetation dynamics under environmental conditions that are fundamentally different from the present. In combination with geochemical and paleobotanical data, the model may help to better constrain the resilience of vegetation-mediated Earth system functions to perturbations in the geologic past and at present.

1 Introduction

Since the emergence of plants on land, vegetation has played a fundamental role in the functioning of the Earth system, controlling the cycling of carbon, oxygen, water and energy on timescales ranging from seconds to millions of years. On short timescales, vegetation-climate interactions include biophysical interactions with the atmosphere, such as the exchange of energy, momentum and water (Boyce and Lee, 2017), or the assimilation and sequestration of carbon in biomass and soils (Sitch et al., 2008). On geologic timescales of millions of years, vegetation interacts with continental erosion and weathering processes, and contributes to the burial of organic material in marine sediments, representing long-term controls of Earth's climate evolution, atmospheric composition and surface structures (Berner, 2004; Dahl and Arens, 2020; Hilton and West, 2020). While controlling the functioning of global biogeochemical cycles, vegetation systems are at the same time highly sensitive to changes in the physical environment. To a certain degree of environmental change, plants can respond through acclimation and variation in the expression of plastic traits (Kristensen et al., 2020; Liu et al., 2024; Wang et al., 2020). More severe and persistent perturbations can trigger large-scale eco-evolutionary dynamics, including range shifts of species tracking their habitats, competition dynamics, and trait evolution due to the continuous selection for individuals that are best adapted to the new conditions (Korasidis et al., 2022; Matthaeus et al., 2023; McElwain et al., 2007; Sitch et al., 2008; Wing et al., 2005). The physical environment and vegetation represent a co-evolutionary system through time. Understanding their dynamic interplay is key to resolving Earth's past and future bioclimatic evolution (Beerling and Berner, 2005; Gurung et al., 2024).

The paleobotanical record offers several examples of how vegetation diversity and functioning have markedly changed during past periods of climatic change (Korasidis et al., 2022; McElwain and Punyasena, 2007; Wing and Currano, 2013; Xu et al., 2022), and similar dynamics are expected under current anthropogenically driven climate change (Etterson and Shaw, 2001; Gonzalez et al., 2010; Sitch et al., 2008). Due to the scarcity of observational data from the deep past, and in order to project how land surface processes and climate will interact in the future, we generally rely on numerical models to simulate the behaviour and interactions between vegetation and other Earth system components (Fisher et al., 2014; Matthaeus et al., 2023; McElwain et al., 2024). Complex models exist to describe communities of plant species and associated biogeochemical and ecological processes (i.e., dynamic vegetation models), which have been fundamental to advancing our understanding of vegetation and climate interactions under global environmental change (Fisher et al., 2014; Sitch et al., 2008). An important drawback of most currently available vegetation models is that they are strongly parametrized around the functioning of plant species and communities under present-day environmental conditions. For example, most dynamic vegetation models represent the global diversity of plant species with a small and fixed number of plant functional types that differ in pre-defined

https://doi.org/10.5194/egusphere-2025-6002
Preprint. Discussion started: 17 December 2025

functional traits and biogeochemical parametrizations (Berzaghi et al., 2020; Fisher et al., 2014). This approach neglects eco-evolutionary dynamics and natural selection that will result in vegetation systems continuously responding and adapting to new environmental conditions (Berzaghi et al., 2020). The static approach of plant functional type analogues is particularly problematic when applying the models to climatic conditions that are fundamentally different from the present, as have occurred during most of Earth's past (Judd et al., 2024), or as we expect under future warmer climates (Fisher et al., 2014; Franklin et al., 2020). It is similarly problematic during past periods when modern-like plant traits and trait combinations had not yet evolved (Matthaeus et al., 2023; White et al., 2020; Wilson et al., 2017). Moreover, an approach that strongly focuses on present-day functioning will limit our ability to understand major co-evolutionary transitions in Earth's past, where both biotic and abiotic environmental changes interactively reshaped the functioning of the Earth system.

A promising approach to increase robustness in the prediction of vegetation functioning under changing environmental conditions is to focus on organizing principles of biological systems (Franklin et al., 2020; Harrison et al., 2021). An organizing principle describes how components of a complex system behave together, rather than characterizing the functioning of the individual components. Natural selection, i.e., the differential survival and reproduction success of individuals in a specific environment, represents such an organizing principle for vegetation systems. All plants that can persist in an environment must have traits that allow them to pass through the filter of natural selection, with abiotic and biotic selection processes eliminating uncompetitive plants. Consequently, trait-environment relationships may be predictable by considering selection to favour plant functional trait combinations that maximize fitness (Franklin et al., 2020; Harrison et al., 2021). Model-based implementations of such eco-evolutionary optimality concepts make use of plant carbon economics with trait and allocation strategies being associated with carbon gains and losses that apply across species. By maximizing a fitness measure, an optimal trait allocation strategy under given environmental conditions can be predicted (Franklin et al., 2020). The two major axes of variation in plant growth forms observed across the globe today include variation in plant size and leaf characteristics (Díaz et al., 2016). Both these functional traits are strongly associated with a plant's carbon balance. Height growth determines the competitiveness in acquiring light resources for carbon assimilation, but is associated with increased construction and maintenance carbon losses (Falster and Westoby, 2003). Variation in leaf characteristics particularly represent the leaf economics spectrum, ranging from species with economically constructed and short-lived "acquisitive" leaves of low leaf mass per area, to species with "conservative" leaves that have longer lifespans and increased persistence under environmental stress but are associated with a reduced carbon sequestration potential (Díaz et al., 2016; Wright et al., 2004). Mechanistic modelling of such carbon economic trade-offs across environmental gradients can resolve major patterns in the global vegetation trait distribution (Franklin et al., 2014, 2020; King, 1990; Rüger et al., 2020; Schymanski et al., 2009; Wang et al., 2023).

Here, we present and evaluate the model TREED (TRait Ecology and Evolution over Deep time), a vegetation model to continuously predict vegetation structure and functioning based on eco-evolutionary optimality principles across timescales from centuries to millions of years. The grid-based vegetation model is built around competing trait allocation strategies that

https://doi.org/10.5194/egusphere-2025-6002
Preprint. Discussion started: 17 December 2025

determine plant fitness under given environmental conditions. It is assumed that adaptation, competition, environmental filtering and evolution result in plants to allocate carbon and traits in a way that maximizes height growth (i.e., light competitiveness), while maintaining a positive carbon balance. With the current set of considered trait trade-offs, the model resolves plant height, leaf longevity, leaf carbon, and phenology (deciduous or evergreen) as the main independent axes of vegetation trait variation. Additional traits and whole-plant architecture are derived using functional and allometric relationships with these main traits, and by considering a generalized plant physiology. With a low model complexity, minimal necessary environmental inputs, and fast computational time, the model is primarily designed to investigate vegetation dynamics in Earth's past and to test a range of eco-evolutionary hypotheses during periods of environmental change. We will describe and evaluate the following main functionalities of the model:

1) Predict the global vegetation structure, trait distribution, and associated carbon fluxes of a vegetation in eco-evolutionary equilibrium with the environment.
2) Predict vegetation structures and functioning during climatic transitions, limited by the capacity of vegetation to adapt traits through evolution or a dispersal-based vegetation redistribution.

Finally, testing the fitness of different functional trait combinations in an environment–as done in TREED–is strongly related to the concept of functional diversity, i.e., the range of functional traits that can be observed within a plant community. Using the generalized plant physiology and continuous trait space of the model, we use it to:

3) Identify locations of a high potential for functional richness and co-existence of variable plant trait combinations. By combining local functional richness and vegetation diversity metrics at the landscape level, we further estimate locations of a high plant biodiversity potential.

2 TREED model description

A TREED model simulation consists of four processes executed in succession (Fig. 1): 1) initialization and allocation of plant functional traits, 2) calculation of carbon and water fluxes, 3) an optimization function to predict the optimal trait distribution under given climatic and topographic conditions, and 4) eco-evolutionary processes including trait evolution and dispersal dynamics that determine the transition speed from a prevailing vegetation trait distribution towards the predicted optimum trait distribution.

TREED is a grid-based vegetation model: every grid cell is associated with a combination of traits that describe a location's vegetation structure. As the model does not explicitly resolve plant individuals, cohorts or populations within the grid cell, the trait values can be considered to describe a community-representative average plant that occupies the entire grid cell. Four key traits fundamentally describe a location's vegetation structure: an individual plant's average leaf carbon pool size during the growing season ($C_{leaf;}$ g C per individual), the community-average plant height ($H;$ m), the dominant phenological strategy (*phenology;* deciduous or evergreen) and the average leaf longevity ($a_{ll;}$ years). Additionally, the vegetation of each location

https://doi.org/10.5194/egusphere-2025-6002
Preprint. Discussion started: 17 December 2025

is associated with a climatic niche that describes bioclimatic limits for productivity. The climatic niche is only considered in transient simulations as described in section 2.4. Based on these key traits and generalized allometric and functional relationships, a range of additional plant characteristics important for vegetation functioning are derived. In each location, the values of the key traits are determined simultaneously in an optimization procedure under consideration of local climatic conditions, searching for the trait combination that maximizes the community average plant height under the constraint of maintaining a positive annual carbon balance (balance between photosynthesis, respiration and tissue turnover carbon investments). Functional trait trade-offs thereby limit the possible trait space to a realistic range. By maximizing the average plant height, the model assumes that plants are in continuous competition for light, and that plant trait combinations that maximize photosynthetic carbon gains and height represent a stable trait strategy that is likely to persist and dominate an ecosystem, as explained in more details in sections 2.3-2.4.

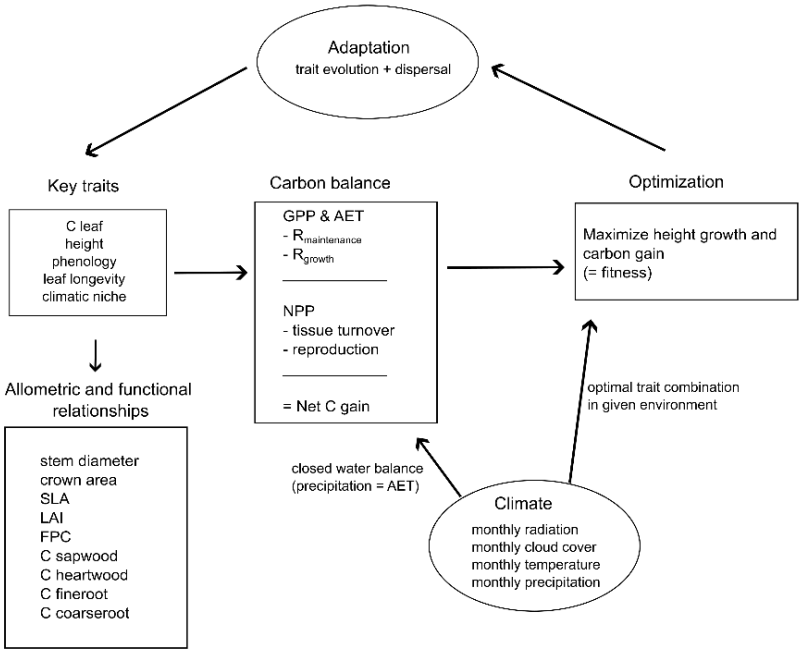

Figure 1: Schematic overview of TREED model processes. C = carbon, SLA = specific leaf area, LAI = leaf area index, FPC = foliage projective cover, GPP = gross primary productivity, AET = actual evapotranspiration, $R_{maintenance}$ = maintenance respiration, R_{growth} = growth respiration, NPP = net primary productivity.

2.1 Allometric and functional relationships

Specific leaf area (*SLA;* $m^2\ g^{-1}$ C) is related to leaf longevity, representing the leaf economics spectrum (Wright et al., 2004), which is based on the observation that plants across growth forms, biomes and climates show a similar range of feasible leaf investment strategies along a gradient from "acquisitive" leaves with high SLA but low leaf longevities, to "conservative"

https://doi.org/10.5194/egusphere-2025-6002
Preprint. Discussion started: 17 December 2025

leaves with low SLA but increased leaf longevity and persistence in harsh environments (Díaz et al., 2016; Wright et al., 2004). The generalized functional relationship used in the TREED model represents an intermediate form of the leaf economic trade-off used for needle-leaved and broadleaved plants with prescribed leaf longevities in the LPJ dynamic vegetation model (Schaphoff et al., 2018; Fig. 2):

$$SLA = (2 \cdot 10^{-4}) \cdot \frac{1}{DM_c} \cdot 10^{2.25 - \log(a_{ll} \cdot 12)} \quad (1)$$

with DM_c being an assumed average dry matter carbon content of 0.47 g C per g of dry matter and a_{ll} the leaf longevity in years. The generalized relationship implies that modelled plants will have leaf longevity and *SLA* combinations in between two endmember strategies: short leaf longevity/high *SLA* strategies, representing broadleaved deciduous or evergreen plants, or long leaf longevity/low *SLA* representing evergreen, needle-leaved plants (Fig. 2). For a given leaf carbon pool, a high *SLA* will result in a high leaf area and light interception potential but is associated with high annual carbon investments to rebuild the leaf carbon pool due to the short leaf longevity. Whether such a strategy is favourable over long leaf longevities and reduced annual leaf carbon investments, as well as the exact duration of the leaf longevity, depend on local climatic conditions (precipitation, radiation and temperature) and is evaluated in the optimization procedure (see section 2.3). By affecting the carbon assimilation potential as well as annual carbon turnover costs, the leaf investment trade-off further contributes to determine whether an evergreen or a deciduous phenology (i.e., no leaves during part of the year) is more favourable under temperate climatic conditions (see section 2.2.3). The consideration of a predicted and continuous range of possible leaf longevities and *SLA* strategies represents an important difference to plant functional type-based vegetation models with prescribed leaf traits.

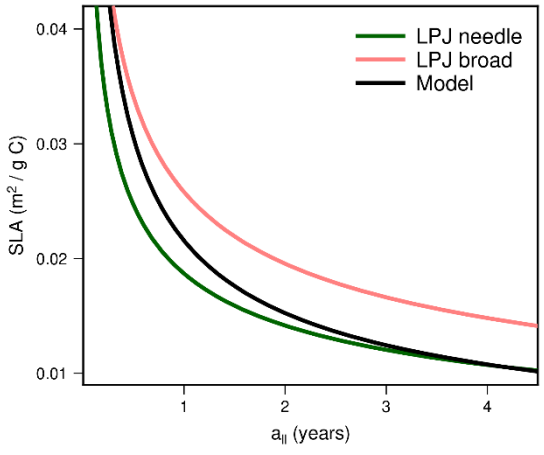

Figure 2: Generalized relationship between leaf longevity (a_{ll}) and specific leaf area (*SLA*). For a given size of the leaf carbon pool, short leaf longevities and high SLA result in a high light interception potential (e.g., total leaf area and leaf area index) but are associated with higher annual carbon investments to rebuild the carbon pool due to the short longevity. The generalized relationship employed in the model represents an intermediate form between the leaf longevity to SLA

https://doi.org/10.5194/egusphere-2025-6002
Preprint. Discussion started: 17 December 2025

relationships considered for specific plant functional types with fixed a_{ll} in the LPJ vegetation model (Schaphoff et al., 2018; Sitch et al., 2003).

Following the allometric scaling relationships from the LPJ vegetation model (Schaphoff et al., 2018; Sitch et al., 2003), the size of a plant individual's average leaf carbon pool (C_{leaf}) and *SLA* determine the average leaf area of a plant (*LA;* m^2):

$$LA = SLA \cdot C_{leaf} \tag{2}$$

Following the pipe model (Shinozaki et al., 1964; Waring et al., 1982), an individual's leaf area and sapwood cross-section area (*SA;* m^2) are assumed proportional (all pre-defined model parameters are listed in Table 1):

$$LA = k_{la:sa} \cdot SA \tag{3}$$

Leaf and fine root carbon allocation ($C_{fineroot}$; g C per individual) are related by a fine root to leaf carbon ration (*r:s;* dimensionless):

$$C_{leaf} = r{:}s \cdot C_{fineroot} \tag{4}$$

Plant height and diameter (*D;* m) are assumed to relate according to (Huang et al., 1992):

$$H = k_{allom2} \cdot D^{k_{allom3}} \tag{5}$$

Further, diameter and crown area (*CA;* m^2) are assumed to scale following:

$$CA = \min(k_{allom1} \cdot D^{k_{rp}}, CA_{max}) \tag{6}$$

with an assumed maximum crown area (CA_{max}) of 15 m^2 (Sitch et al., 2003). The *CA* represents the average surface area occupied by a single average plant in a model grid cell.

An average plant's individual leaf area index ($LAI_{individual}$; $m^2\ m^{-2}$) can be calculated as:

$$LAI_{individual} = \frac{C_{leaf} \cdot SLA}{CA} \tag{7}$$

It is assumed that grid cells are fully covered by the local average plant that is characterised by the five key traits (Fig 1). Assuming no canopy overlap, the number of plant individuals per grid cell ($N_{individuals}$) is thus $N_{individuals} = \frac{cell\ area}{CA}$. Consequently, the grid cell's leaf area index (*LAI*), is equal to the leaf area index of the average individual ($LAI = LAI_{individual}$):

$$LAI = \frac{LA_{individual} \cdot N_{individuals}}{cell\ area} = \frac{LA_{individual}}{CA} = LAI_{individual} \tag{8}$$

The light interception potential within a grid cell, i.e., the fraction of photosynthetically active radiation absorbed by leaves (*fAPAR;* dimensionless), is estimated using the Lambert-Beer law:

https://doi.org/10.5194/egusphere-2025-6002
Preprint. Discussion started: 17 December 2025

$$fAPAR = 1 - e^{-k \cdot LAI} \quad (9)$$

Thereby, we account for a tendency of an increased light extinction coefficient (k) for broadleaved, short-lived and high *SLA* leaves compared to needle-leaved, long-lived and low *SLA* leaves (Zhang et al., 2014), by linearly relating k in the range between 0.6 and 0.4 to the average leaf longevity, according to:

$$k = 0.6 - 0.04 \cdot a_{ll} \quad (10)$$

A plant's sapwood carbon pool ($C_{sapwood}$; g C per individual) is derived from the plant's sapwood cross section area and height, assuming a cylindrical geometry and a constant wood density (WD; g C m^{-3}):

$$C_{sapwood} = SA \cdot H \cdot WD \quad (11)$$

The model considers a globally generalized plant physiology, and it is therefore assumed that for small plants that would not be considered trees, $C_{sapwood}$ describes an overall structural carbon pool that is proportional to a plant's height.

Woody tissue represents the by far most important component of global above ground biomass (Brunner and Godbold, 2007). Therefore, a generalized power law derived from global canopy height (Lang et al., 2023) and above ground biomass density estimates (Huang et al., 2021; Santoro et al., 2010) is used to describe the relationship between the modelled volume of an average plant in a grid cell ($H \cdot CA$) and total stem biomass ($C_{stem} = C_{sapwood} + C_{heartwood}$):

$$C_{stem} = k_{int} \cdot (CA \cdot H)^{k_{pow}} \quad (12)$$

Coarse root carbon ($C_{coarseroot}$; g C per individual) is assumed to be around a fourth of the stem biomass, as estimated from current above ground and below ground biomass data (Huang et al., 2021):

$$C_{coarseroot} = 0.25 \cdot (C_{heartwood} + C_{sapwood}) \quad (13)$$

All allometric constants (k_{allom1}, k_{allom2}, k_{allom3}, k_{rp}, $k_{la:sa}$, $k_{intercept}$, k_{pow}) were calibrated using present-day canopy height and above ground biomass data and are listed in Table 1. The resulting height to biomass relationship is shown in the model evaluation section 5.3.

Table 1: Pre-defined TREED model parameters required to approximate vegetation structure, photosynthesis, respiration, carbon turnover and trait evolution. Dimensionless parameters indicated by [-].

Function	Parameter	Description	Value
Allometric relationships			
	$k_{la:sa}$	Leaf area to sapwood cross-section area	4000 [-]
	k_{allom2}	Height-diameter relationship	50 [-]
	k_{allom3}	Height-diameter relationship	0.6 [-]
	k_{allom1}	Diameter-crown area relationship	75 [-]
	k_{rp}	Diameter-crown area relationship	1.6 [-]
	DM_c	Average dry biomass carbon content	0.47 g C / g dry biomass

https://doi.org/10.5194/egusphere-2025-6002
Preprint. Discussion started: 17 December 2025

	WD	Average wood density	250000 g C / m^3
	k_{int}	Volume-biomass relationship	194 g biomass / m^3
	k_{pow}	Volume-biomass relationship	1.23 [-]
	r:s	Fumeroot to leaf carbon ratio	1 [-]
Carbon balance			
	$\alpha_{leaf:stand}$	Leaf to stand radiation use efficiency scaling	0.55 [-]
	α_{C3}	Intrinsic quantum efficiency for CO_2 uptake	0.08 [-]
	τ_{25}	Rubisco specifity at 25°C	2600 [-]
	$q_{10\tau}$	Rubisco temperature sensitivity parameter	0.57 [-]
	K_C	Michaelis-Menten constant for CO_2	30 Pa
	K_O	Michaelis-Menten constant for O_2	30000 Pa
	$[O_2]$	Partial pressure of O_2 (default)	20900 Pa
	b	Leaf respiration coefficient	0.015 per day
	θ	Light and Rubisco co-limitation shape factor	0.7 [-]
	λ_{max}	Maximum leaf-atmosphere gas exchange	0.8 [-]
	g_{min}	Minimum canopy conductance	0.3 mm / s
	r	Base respiration rate	0.066 g C / g N / day
	$C:N_{sapwood}$	C to N ratio woody tissue	330 [-]
	$C:N_{root}$	C to N ratio root tissue	29 [-]
	r_{gr}	Growth respiration fraction	0.25 [-]
	r_{repr}	C allocation to reproduction (fraction of NPP)	0.1 [-]
	$f_{sapwood}$	Sapwood carbon turnover time	1/15 per year
	$f_{heartwood}$	Heartwood carbon turnover time	1/15 per year
	$f_{coarseroot}$	Coarseroot carbon turnover time	1/15 per year
Trait dynamics			
	α	Rate of trait adaptation per time step	0 to 1 [-]
	$k_{nichebreath}$	Impact of climate niche deviation (default)	0.02

2.2 Carbon balance

2.2.1 Photosynthesis and evapotranspiration

Based on the derived characteristics of the vegetation at a location, photosynthetic carbon assimilation, growth and maintenance respiration, and tissue turnover carbon investments are calculated. The following carbon and water flux calculations are adapted from the LPJ vegetation model (Schaphoff et al., 2018; Sitch et al., 2003), with photosynthesis being modelled using the Farquhar photosynthesis model (Farquhar et al., 1980; Farquhar and Caemmerer, 1982) and under consideration of the generalizations for global modelling by Collatz et al., (1991). The "strong optimality" hypothesis (Haxeltine and Prentice, 1996b) is applied, assuming that nitrogen content and Rubisco activity of leaves vary seasonally and with canopy position in a way to maximize the net assimilation at the leaf level. The resulting model has the form of a light-use efficiency model, depending on the photosynthetically active radiation (*PAR*), temperature, daylength and water availability.

Half of the downwelling shortwave radiation at the surface (*RSDS;* MJ m^{-2} day^{-1}) is assumed photosynthetically active radiation (*PAR;* MJ m^{-2} day^{-1}):

$$PAR = 0.5 \cdot RSDS \quad (14)$$

https://doi.org/10.5194/egusphere-2025-6002
Preprint. Discussion started: 17 December 2025

The fraction of *PAR* absorbed by the local vegetation (*APAR;* MJ m^{-2} day^{-1}) is calculated considering a grid cell's *fAPAR*, a leaf to stand level scaling factor ($\alpha_{leaf:stand}$; dimensionless), and a climate niche suitability factor ($\Phi_{nichestress}$; dimensionless):

$$APAR = PAR \cdot fAPAR \cdot \alpha_{leaf:stand} \cdot \Phi_{nichestress} \quad (15)$$

The climate niche suitability factor is an introduced variable that will be described in further detail in section 2.4 and that is only important in non-steady state TREED simulations, considering eco-evolutionary adaptation dynamics between different climate states. The leaf to stand scaling factor accounts for reductions in *PAR* utilization at the stand level in natural ecosystems (Haxeltine and Prentice, 1996b).

Photosynthesis is calculated as the minimum of light-limited (J_E; mol C m^{-2} h^{-1}) and Rubisco-limited photosynthesis (J_C; mol C m^{-2} h^{-1}) (Haxeltine and Prentice, 1996a). Light-limited photosynthesis is calculated as:

$$J_E = C_1 \cdot \frac{APAR}{daylength} \quad (16)$$

Where *daylength* (h) is the number of sunshine hours per day, depending on the day of the year and geographic latitude, and

$$C_1 = \alpha_{C_3} \cdot f_{temp} \cdot \left(\frac{p_i - \Gamma_*}{p_i + 2 \cdot \Gamma_*}\right) \quad (17)$$

With p_i (Pa) being the leaf internal partial pressure of CO_2, calculated as $p_i = \lambda \cdot p_a$, where p_a (Pa) is the ambient partial pressure of CO_2 and λ (dimensionless; between 0 and 0.8) describes the leaf-atmosphere water and carbon exchange. The latter depends on the local water availability and vegetation stomatal opening, determining the concentration ratio between intercellular and ambient CO_2. The α_{C_3} (dimensionless) in eq. (17) is the intrinsic quantum efficiency for CO_2 uptake of C_3 plants. In the current model version only C_3 physiology is considered. The factor f_{temp} (dimensionless) describes a general temperature dependency of the efficiency of the photosynthetic pathway, adapted from Schaphoff et al., (2018) and generalized for all plants as:

$$f_{temp,low} = \frac{1}{(1+\exp(0.25 \cdot (12 - T)))} \quad (18)$$

$$f_{temp,high} = 1 - \frac{1}{1+\exp(-(T - 40.85))} \quad (19)$$

$$f_{temp} = f_{temp,low} \cdot f_{temp,high} \quad (20)$$

with T being the monthly average temperature. Accordingly, f_{temp} indicates an inhibition of photosynthesis for monthly average temperatures below 0 °C and higher than 45 °C, and an optimum photosynthetic rate between 25-30 °C. Finally, Γ_* in eq. (17) represents the photorespiratory CO_2 compensation point:

$$\Gamma_* = \frac{[O_2]}{2 \cdot \tau} \quad (21)$$

https://doi.org/10.5194/egusphere-2025-6002
Preprint. Discussion started: 17 December 2025

with $\tau = \tau_{25} \cdot q_{10_\tau}^{\frac{T-25}{10}}$ (dimensionless) being the specificity factor that reflects the ability of Rubisco to discriminate between CO_2 and O_2. $[O_2]$ is the partial pressure of oxygen (Pa), τ_{25} is the τ value at 25 °C, and q_{10_τ} a temperature sensitivity parameter.

The Rubisco-limited photosynthesis is calculated as:

$$J_C = C_2 \cdot V_m \tag{22}$$

with

$$C_2 = \frac{p_i - \Gamma_*}{p_i + K_c \cdot \left(1 + \frac{[O_2]}{K_O}\right)} \tag{23}$$

where K_C and K_O are Michaelis-Menten constants for CO_2 and O_2, respectively. V_m (mol C m^{-2} day^{-1}) represents the maximum Rubisco capacity which is derived from optimizing the daily net photosynthesis at the leaf level with respect to V_m ($\frac{\partial A_{nd}}{\partial V_m} = 0$, where $A_{nd} = A_{gd}$-R_{leaf}; Haxeltine and Prentice, 1996b) resulting in:

$$V_m = \frac{1}{b} \cdot \frac{C_1}{C_2} \cdot \left((2 \cdot \theta - 1) \cdot s - (2 \cdot \theta \cdot s - C_2) \cdot \sigma\right) \cdot APAR \tag{24}$$

where b (day^{-1}) is a static leaf respiration coefficient, θ (dimensionless) a shape parameter that describes the co-limitation of light and Rubisco activity (Haxeltine and Prentice, 1996a), and

$$\sigma = \sqrt{1 - \frac{C_2 - s}{C_2 - \theta \cdot s}} \tag{25}$$

and

$$s = \frac{24}{daylength} \cdot b \tag{26}$$

The maximum Rubisco capacity is calculated under the assumption of no water limitation, thus $\lambda = \lambda_{max}$.

Daily gross photosynthesis (A_{gd}; g C m^{-2} $daytime^{-1}$) is calculated as

$$A_{gd} = \frac{(J_E + J_C - \sqrt{(J_E + J_C)^2 - 4 \cdot \theta \cdot J_E \cdot J_C})}{2 \cdot \theta} \cdot daylength \tag{27}$$

Subtracting the daytime leaf respiration results in the daily net daytime photosynthesis (A_{dt}; g C m^{-2} $daytime^{-1}$):

$$A_{dt} = A_{gd} - \left(\frac{daylength}{24}\right) \cdot R_{leaf} \tag{28}$$

With R_{leaf} (g C m^{-2} day^{-1}) being the leaf dark respiration. Leaf dark respiration is expected to be predominantly driven by the turnover of Rubisco proteins for photosynthesis and thus, closely scales with the maximum Rubisco capacity (Schaphoff et al., 2018; Wang et al., 2020):

https://doi.org/10.5194/egusphere-2025-6002
Preprint. Discussion started: 17 December 2025

$$R_{leaf} = V_m \cdot b \tag{29}$$

The photosynthetic carbon assimilation rate is related to the canopy conductance of water vapor (g_c; mm s^{-1}) through the CO_2 diffusion gradient between the intercellular airspace and the atmosphere, according to:

$$g_c = \frac{1.6 \cdot A_{dt}}{p_a \cdot (1-\lambda)} + g_{min} \tag{30}$$

Where g_{min} (mm s^{-1}) is a minimum canopy conductance that occurs due to non-photosynthesis related processes. The maximum possible canopy conductance is limited by the local water availability. The exchange of water and carbon with the atmosphere is controlled by the parameter λ, with high λ describing non-water limited conditions and maximum water and carbon exchange, whereas low λ indicates stomatal closure and limited gas exchange. Eq. (30) therefore relates stomatal opening, canopy conductance and photosynthetic rate. A potential water limitation is evaluated by comparing the vegetation's water demand (E_{demand}; mm day^{-1}) and transpiration, with the supply of water, constrained by:

$$E_{supply} = \min(E_{max}, P_{mean}) \tag{31}$$

where E_{max} represents a maximum daily canopy-scale transpiration rate of 5 mm day^{-1} (Sitch et al., 2003), and P_{mean} is the average daily precipitation rate in mm day^{-1}.

Following Schaphoff et al., (2018) and Monteith (1995), E_{demand} is calculated as:

$$E_{demand} = E_{eq} \cdot \frac{\alpha_m}{1+\frac{g_m}{g_c}} \tag{32}$$

Employing a maximum Priestley-Taylor coefficient α_m of 1.391, and a conductance scaling factor g_m of 3.26 mm s^{-1}. E_{eq} is the equilibrium evapotranspiration rate calculated as:

$$E_{eq} = \frac{sa}{sa+\gamma} \cdot \frac{R_n}{\lambda_{vap}} \tag{33}$$

with sa (Pa K^{-1}) being the slope of the saturation vapor pressure curve, γ (J kg^{-1}) the psychrometric constant, R_n (J m^{-2} day^{-1}) the daytime net radiation and λ_{vap} (J kg^{-1}) the latent heat of vaporization.

To evaluate a potential water limitation, E_{demand} is first calculated using $\lambda = \lambda_{max}$, representing the water demand under maximum potential canopy conductance. In case the resulting E_{demand} is lower than the available water (E_{supply}), λ is kept at the maximum level resulting in carbon and water being exchanged at the maximum level possible for the local vegetation. In case the canopy conductance calculated with $\lambda = \lambda_{max}$ results in $E_{demand} > E_{supply}$, a bisection algorithm is employed to find a canopy-atmosphere gas exchange parameter $\lambda < \lambda_{max}$ that satisfies Eqs. (28) and (26), and that results in a closed water balance ($E_{demand} = E_{supply}$), solving for:

$$0 = A_{dt} - A_{dt} = A_{gd} - \left(\frac{daylength}{24}\right) \cdot R_{leaf} - p_a \cdot (g_c - g_{min}) \cdot \frac{(1-\lambda)}{1.6} \tag{34}$$

https://doi.org/10.5194/egusphere-2025-6002
Preprint. Discussion started: 17 December 2025

For computational efficiency, the bisection algorithm is simplified to evaluating eq. (34) at 12 pre-defined levels for λ between 0 and 0.8 and choosing the λ value resulting in the closest value to zero.

Following Sitch et al., (2003), actual evapotranspiration (*AET;* mm day^{-1}) is then calculated as

$$AET = \min\left(E_{supply}, E_{demand}\right) \tag{35}$$

with only water effectively being transpired contributing to *AET* in case $E_{demand} < E_{supply}$.

2.2.2 Respiration

Metabolically active plant tissues are associated with maintenance respiration. While the leaf respiration is calculated based on the maximum Rubisco activity (eq. 29), sapwood ($R_{sapwood}$; g C m^{-2} day^{-1}) and fine root respiration ($R_{fineroot}$; g C m^{-2} day^{-1}) are calculated following Schaphoff et al., 2018, as:

$$R_{sapwood} = r \cdot AF \cdot \frac{C_{sapwood}}{C{:}N_{wood}} \cdot g(T_{air}) \tag{36}$$

$$R_{fineroot} = r \cdot AF \cdot \frac{C_{fineroot}}{C{:}N_{root}} \cdot g(T_{soil}) \tag{37}$$

where r (g C (g N)$^{-1}$ day^{-1}) is a base respiration rate, $C{:}N_{wood}$ (dimensionless) and $C{:}N_{root}$ (dimensionless) are the C:N ratios in wood and root tissue, respectively. Plants from warm environments have consistently lower respiration rates than plants from cold environments (Reich et al., 2016; Sitch et al., 2003; Zhu et al., 2021). To account for this apparent downregulation of base respiration rates under warmer temperatures while not using fixed functional type-based respiration rates in the model, *AF* (dimensionless) is an introduced arbitrary acclimation factor that is 1 for environments with monthly average temperatures below 10 °C, 0.3 for average temperatures higher than 30 °C and

$$AF = 1.35 - 0.035 \cdot T \tag{38}$$

for intermediate temperatures. Finally, $g(T_{air})$ and $g(T_{soil})$ (dimensionless) describe the temperature dependency of respiration using a modified Arrhenius equation that accounts for declining respiration rates with temperatures (Lloyd and Taylor, 1994; Schaphoff et al., 2018; Sitch et al., 2003):

$$g(T) = \exp\left(308.56 \cdot \left(\frac{1}{56.02} - \frac{1}{T+46.02}\right)\right) \tag{39}$$

where T (°C) is either the monthly average air temperature for $g(T_{air})$, or the monthly average soil temperature for $g(T_{soil})$. The monthly average soil temperature is approximated from the air temperature, assuming the same annual mean but a damped seasonal cycle:

$$T_{soil} = T_{mean} + \left(\frac{T - T_{mean}}{2}\right) \tag{40}$$

https://doi.org/10.5194/egusphere-2025-6002
Preprint. Discussion started: 17 December 2025

with T_{mean} being the annual average temperature.

2.2.3 Annual carbon balance

With the model using monthly average values of temperature, precipitation, radiation and cloud cover as inputs, all above-described daily carbon fluxes are calculated as monthly average values and are then integrated over the course of the year. Accordingly,

$$GPP = \sum_{i=1}^{12} A_{gd,i} \cdot mdays_i \tag{41}$$

with i being the month of the year, and $mdays_{,i}$ the number of days of month i.

For deciduous plants in temperate regions (see section 2.3), the leaf longevity limits the duration of the growing season. For these locations, fluxes are calculated and integrated over the warmest months of the year up to the duration of the leaf longevity. The annual net primary productivity (*NPP;* g C m^{-}2 year^{-1}) is calculated as:

$$NPP = \left(1 - r_{gr}\right) \cdot \left(GPP - R_{leaf} - R_{sapwood} - R_{fineroot}\right) \tag{42}$$

where r_{gr} (dimensionless) accounts for a fixed fraction of the assimilated carbon assumed to be invested for growth respiration (Schaphoff et al., 2018; Sitch et al., 2003).

Being a grid-based model, TREED describes the structure and functioning of an average plant representing the locally dominating vegetation growth form. The model does not explicitly resolve establishment, growth and mortality of individuals. Instead, to evaluate whether a growth from (e.g., height, size of carbon pools, leaf characteristics) is suitable for a location, an area-based annual carbon balance is calculated. Based on the longevity associated with the local vegetation's carbon pools, it is estimated how much carbon is invested annually to rebuild and maintain the local vegetation. For a vegetation form or trait combination to establish and survive at a location, the area-based annual average regrowth carbon costs cannot exceed the average net carbon sequestration potential (NPP). Average yearly tissue turnover carbon costs (F in g C m^{-2} year^{-1}) of sapwood, heartwood and coarse roots are calculated assuming constant, tissue-specific turnover rates (Table 1):

$$F_{sapwood} = C_{sapwood} \cdot f_{sapwood} \cdot \frac{1}{CA} \tag{43}$$

$$F_{heartwood} = C_{heartwood} \cdot f_{heartwood} \cdot \frac{1}{CA} \tag{44}$$

$$F_{coarseroot} = C_{coarseroot} \cdot f_{coarseroot} \cdot \frac{1}{CA} \tag{45}$$

The fine root and leaf carbon turnover costs depend on the plant's phenology and leaf longevity (in years):

$$F_{leaf} = \begin{cases} C_{leaf} \cdot \frac{1}{a_{ll}} \cdot \frac{1}{CA} & evergreen \\ C_{leaf} \cdot 1\ year^{-1} \cdot \frac{1}{CA} & deciduous \end{cases} \tag{46}$$

https://doi.org/10.5194/egusphere-2025-6002
Preprint. Discussion started: 17 December 2025

Fine root turnover is assumed proportional to the leaf longevity (Schaphoff et al., 2018), with a minimum fine root longevity of one year:

$$F_{fineroot} = \begin{cases} C_{fineroot} \cdot \frac{1}{a_{ll}} \cdot \frac{1}{CA} & a_{ll} > 1 \\ C_{fineroot} \cdot 1\ year^{-1} \cdot \frac{1}{CA} & a_{ll} \leq 1 \end{cases} \quad (47)$$

The annual net carbon gain (*NCG;* g C m^{-2} $year^{-1}$) represents the annual average carbon balance of the local vegetation and is calculated as:

$$NCG = \left(1 - r_{repr}\right) \cdot NPP - F_{leaf} - F_{fineroot} - F_{sapwood} - F_{heartwood} - F_{coarseroot} \quad (48)$$

Where r_{repr} (= 0.1; dimensionless) represents a fixed fraction of the annual NPP allocated to reproduction (Sitch et al., 2003). Only trait combinations resulting in $NCG \geq 0$ are plausible trait combinations in a given environment, ensuring that the local average carbon assimilation is sufficient to build and maintain the vegetation's carbon pools.

2.3 Trait optimization and prediction

Our generalized plant physiology (2.1) and carbon flux calculations (2.2) allow us to calculate a carbon balance for variable combinations of the traits C_{leaf}, H, a_{ll} and *phenology* (deciduous or evergreen). Following optimality principles (Franklin et al., 2020; Harrison et al., 2021), we assume that competition, environmental filtering and natural selection will result in traits of an average individual at a location to evolve towards combinations that maximize fitness. We define fitness as the potential for height growth while maintaining a positive *NCG*. The choice of height as the fitness measure assumes that plants in a community are in continuous competition for light as a major limiting resource, resulting in increased height being associated with a competitive advantage. It is important to note that this approach represents a fitness measure at the community level and not a single-plant optimization, considering that carbon investments into structural tissues in the absence of competitors may not represent an optimal strategy. It can be assumed that height as fitness measure results in an approximation of an evolutionary stable strategy, resulting in a trait combination that is likely stable and dominant in a given climatic environment (Franklin et al., 2020; Valentine and Mäkelä, 2012). Height growth is a compound trait, and its optimization implies finding a leaf longevity, phenology and carbon allocation strategy that maximizes photosynthetic carbon gains over losses through growth and maintenance respiration, as well as tissue turnover carbon costs, all of which increase with increasing height. To predict the trait combination of C_{leaf}, H, a_{ll} and *phenology* that maximize height subject to $NCG \geq 0$ under given climatic conditions, an Evolutionary Centers optimization algorithm from the Julia package Metaheuristics.jl (Mejía-de-Dios and Mezura-Montes, 2022) is employed, with the target function being:

$$minimize\ f\left(C_{leaf}, H, a_{ll}, phenology, climate\right) = |NCG| - \omega \cdot H \quad (49)$$

where ω (= 10) is an arbitrary weighting parameter to ensure stable solutions. By minimizing $|NCG|$, the model will approximate a steady state vegetation at maximum height, i.e., the height at which carbon gains from photosynthesis are

https://doi.org/10.5194/egusphere-2025-6002
Preprint. Discussion started: 17 December 2025

balanced by carbon costs from respiration and turnover. Whether height growth is maximized under a deciduous or evergreen phenology is only evaluated in locations with more than three months with average temperatures below 3 °C, which is considered a necessary condition for a deciduous phenology.

2.4 Eco-evolutionary adaptation dynamics

The TREED modules described under 2.1-2.3 can be used as a stand-alone model to obtain a prediction of vegetation that is in eco-evolutionary equilibrium with the environment, i.e., every grid cell is occupied by vegetation with a stable trait combination that maximizes height. Alternatively, the model can also be used to track vegetation structural and functional changes through time while adapting from a starting state and trait distribution to the predicted optimum state under new or changing climatic conditions. Two pathways of vegetation adaptation are represented: adaptation through evolution of traits and adaptation through dispersal and a redistribution of traits.

2.4.1 Adaptation through evolution

In the trait evolution module, it is assumed that average traits at a location will incrementally evolve towards the trait combination that is predicted as optimal. The rate of trait change is a user-defined adaptation rate α. The rate α is a unitless fraction, resulting in larger changes of traits for larger deviations between the current trait values and the optimal trait values, representing an increased adaptation and selection pressure. Adaptation is considered to represent a range of possible adaptation processes including acclimation, phenotypic plasticity or actual adaptive evolutionary processes that will be particularly relevant on longer timescales. The evolution of C_{leaf}, and a_{ll} is represented as:

$$C_{leaf,evolved} = C_{leaf,previous} + \alpha \cdot \left(C_{leaf,optimized} - C_{leaf,previous}\right) \quad (50)$$

$$a_{ll,evolved} = a_{ll,previous} + \alpha \cdot \left(a_{ll,optimized} - a_{ll,previous}\right) \quad (51)$$

With $C_{leaf,evolved}$ and $a_{ll,evolved}$ representing the new trait values, $C_{leaf,previous}$ and $a_{ll,previous}$ representing the starting trait values, and $C_{leaf,optimized}$ and $a_{ll,optimized}$ representing the target trait values derived from the optimization. The evolution of *phenology* is linked to the leaf longevity trait $a_{ll,evolved}$ and will be deciduous in an environment where a deciduous phenology is possible (at least three months with average temperatures lower than 3 °C) and $a_{ll,optimized}$ and $a_{ll,evolved}$ are less than a year.

In eco-evolutionary mode, the *climatic niche* is taken into consideration as an additional vegetation trait. This trait accounts for the fact that plant species generally exhibit highly conserved climatic niches, which will affect their geographic distribution and productivity potential (Jezkova and Wiens, 2016; Liu et al., 2020; Martínez-Meyer and Peterson, 2006). As part of the vegetation trait set of any location in the model, the climatic niche is described by $T_{min,veg}$, $T_{max,veg}$, $T_{mean,veg}$, representing the coldest month average temperature, warmest month average temperature and mean annual temperature of the environment to which the local vegetation is best adapted to. At initialization of the model, $T_{min,veg}$, $T_{max,veg}$, $T_{mean,veg}$, are set equal to the coldest

https://doi.org/10.5194/egusphere-2025-6002
Preprint. Discussion started: 17 December 2025

month, warmest month and annual average temperature of the local environment, assuming an optimal adaptation to the local climate conditions. If the climatic conditions at a location change, deviations between the local temperature conditions and the climatic niche of the local vegetation will result in a biotic stress, represented as:

$$\Phi_{heat} = \exp\left(-k_{nichebreadth} \cdot \left(T_{max,local} - T_{max,veg}\right)^2\right) \quad if\ T_{max,local} \geq T_{max,veg} \tag{52}$$

$$\Phi_{cold} = \exp\left(-k_{nichebreadth} \cdot \left(T_{min,local} - T_{min,veg}\right)^2\right) \quad if\ T_{min,local} \leq T_{min,veg} \tag{53}$$

$$\Phi_{mean} = \exp\left(-k_{nichebreadth} \cdot \left(T_{mean,local} - T_{mean,veg}\right)^2\right) \tag{54}$$

$$\Phi_{nichestress} = \min\left(\Phi_{heat}, \Phi_{cold}, \Phi_{mean}\right) \tag{55}$$

where $k_{nichebreadth}$ describes the impact of a deviation of the local temperature distribution from the vegetation's climatic niche and can be considered a description of the width of the fundamental niche of the modelled vegetation. The default value for $k_{nichebreadth}$ is set to 0.02, resulting in a decline in productivity for temperature deviations between the coldest month, warmest month or average temperature from the vegetation's climatic niche up to ~15 °C, at which a total loss of productivity occurs. The default niche width of 15 °C approximates the variation in the coldest month, warmest month and average temperature variation observed in present-day biomes (i.e., Koeppen belts) (Beck et al., 2018). The $\Phi_{nichestress}$ affect the photosynthetic potential by limiting the light interception potential in Eq. 15. The $\Phi_{nichestress}$ will particularly start to affect productivity levels if climatic changes reach a magnitude at which a redistribution of vegetation between surrounding grid cells cannot compensate for a loss of adaptation (see section 2.4.2 regarding dispersal).

Like the other vegetation traits, the climatic tolerances of the local vegetation are subject to adaptation through time, evolving towards the local climatic conditions and thereby reducing the biotic stress:

$$T_{min,veg,evolved} = T_{min,veg,previous} + \alpha \cdot \left(T_{CM,local} - T_{min,veg,previous}\right) \tag{56}$$

$$T_{max,veg,evolved} = T_{max,veg,previous} + \alpha \cdot \left(T_{WM,local} - T_{max,veg,previous}\right) \tag{57}$$

$$T_{mean,veg,evolved} = T_{mean,veg,previous} + \alpha \cdot \left(T_{local} - T_{mean,veg,previous}\right) \tag{58}$$

with $T_{CM,local}$ being the local coldest month temperature, $T_{WM,local}$ being the local warmest month temperature and T_{local} the local annual average temperature.

The height trait H is not subject to evolution but is obtained based on the evolved trait set and by evaluating the maximum potential height with the new trait combination using a bisection algorithm that solves for:

$$NCG\left(H, C_{leaf,evolved}, a_{ll,evolved}, phenology_{evolved}, T_{min,veg,evolved}, T_{max,veg,evolved}, T_{mean,veg,evolved}\right) = 0 \tag{59}$$

https://doi.org/10.5194/egusphere-2025-6002
Preprint. Discussion started: 17 December 2025

2.4.2 Adaptation through dispersal

Vegetation can adapt to new climatic conditions not only through trait adaptation but also through range shifts and dispersal. In TREED, a dispersal-based trait redistribution is represented as a moving window operation. Thereby, for each grid cell of the model and for each trait that is also subject to evolution (C_{leaf}, a_{ll}, *phenology*, $T_{min,veg}$, $T_{max,veg}$, $T_{mean,veg}$) a user-defined geographic radius is searched to assess whether there is any current trait value within this radius that is closer to the predicted optimum trait value for the considered location. This approach assumes that the trait values observed within the defined geographic region or moving window represent a trait space and that all possible trait combinations from this trait space are likely to occur in the location of interest. The model's dispersal implementation may overestimate dispersal because it does not consider productivity levels of the dispersing plants, meaning that severely stressed plants are equally likely to disperse the same distance as highly productive plants. The model does also not have a treatment for approximating dispersal vectors, such as wind, insects or animals.

As for evolution, to ensure plausible trait combinations and whole plant architecture, the trait H is not subject to the dispersal dynamics but is obtained by evaluating the maximum potential height at a location given the new trait combination after dispersal (eq. 59).

2.4.3 Eco-evolutionary adaptation dynamics across timescales

The time stepping scheme of TREED is flexible and depends on the inputs of the user (Fig. 3). To complete one evaluation of TREED and to obtain an estimation of the potential vegetation height, leaf characteristics, biomass, carbon and water fluxes of a vegetation in equilibrium with the climatic conditions (i.e., the optimum trait landscape), one year of monthly average climate inputs is needed (i.e., temperature, precipitation, radiation and cloud cover). These monthly average values can represent average values of a specific year or could represent multiyear monthly average values to obtain an average estimate. Similarly, the time stepping in the eco-evolutionary mode is flexible. The time difference between the climatic inputs used to run TREED in the eco-evolutionary mode that considers adaptation dynamics and limitations could range from one year to a million years. The adaptation parameter α, describing a rate of trait change per timestep, and the size of the dispersal search window can be adjusted according to the timescale of interest. It should however be noted that the trait values resolved in TREED and derived using the optimization procedure represent long-term stable, community-representative average plants per grid cell, and adaptation represents changes in this mean vegetation state through time. Consequently, the model does not resolve short-term transient dynamics in the form of population dynamics.

https://doi.org/10.5194/egusphere-2025-6002
Preprint. Discussion started: 17 December 2025

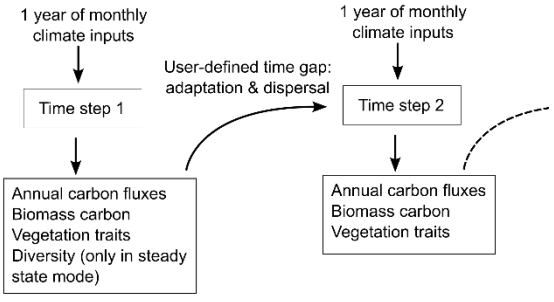

Figure 3: Illustration of time stepping scheme in the TREED model. The model calculates annual carbon fluxes and considers dispersal- and adaptation-based trait changes across a user-defined time gap. Diversity metrics are only calculated in the steady-state mode assuming optimal adaptation, not considering dispersal and evolution dynamics.

3 Estimation of functional richness and diversity potential using TREED

The generalized plant physiology and continuous trait space of TREED allows to assess the performance of variable combinations of the traits C_{leaf}, H, a_{ll}, *phenology* in a specific climatic environment. This cannot only be used to evaluate the fittest trait combination for the environment as explained in section 2.3, but also to generally assess the range of trait combinations that could potentially occur. In TREED, an estimate of the functional richness potential of a location can be obtained by evaluating the carbon balance of a user-defined number of combinations of the traits C_{leaf}, H, a_{ll} covering a wide possible range in these trait values. The model-predicted functional diversity index (*FDI*) represents the number of evaluations resulting in a positive *NCG* (viable growth strategy) from the total number of evaluations (N):

$$FDI = \frac{\#\{i \mid NCG(C_{leaf}, a_{ll}, H) > 0\}}{N} \quad (60)$$

FDI gives an estimate of the diversity potential within a single cell of the model domain and can be interpreted as the carrying capacity of the location, i.e., the range of growth forms that can be supported with the given environmental resources. To avoid an overprediction of functional diversity, the tested trait space should be chosen large and identical for comparisons between model simulations.

Highest levels of plant species richness are observed in regions of high geographic complexity, with heterogeneity of habitats and climatic environments promoting biodiversity by increasing the niche space, refuges, opportunities for isolation and divergent adaptation (Antonelli et al., 2018; Stein et al., 2014). In TREED, a landscape-level diversity potential can be estimated by combining *FDI* at the cell-level with two additional metrics of landscape complexity that resolve the variability and arrangement of vegetation habitats at a larger spatial scale. The landscape heterogeneity index (*LHI*) represents the number of different plant habitats within a moving-window of a user-defined radius (default = 300 km). For the calculation of *LHI*, a categorization of the vegetation distribution in steady state with the climate is conducted. The discrete categories of vegetation

https://doi.org/10.5194/egusphere-2025-6002
Preprint. Discussion started: 17 December 2025

habitat classes are derived from the *H*, a_{ll}, C_{leaf}, *phenology* of the predicted local dominating trait combination, considering 6 height classes (0-5 m, 5-10 m, 10-20 m, 20-30 m, 30-40 m, >40 m), 6 leaf longevity classes (0-0.5, 0.5-1, 1-2, 2-3, 3-4, >4 years), 6 leaf carbon pool classes (0-500, 500-1000, 1000-2000, 2000-3000, 3000-4000, >4000 g C per individual) and two phenology classes (deciduous or evergreen), resulting in a total of 432 discrete classes. *LHI* is then calculated as the number of different vegetation habitat classes within a moving window relative to the maximum number of different vegetation classes that could occur within this window (i.e., every grid cell is occupied by a different vegetation class):

$$LHI = \frac{\#\ of\ distinct\ vegetation\ classes}{\#\ of\ cells\ in\ considered\ window} \tag{61}$$

Additionally, the degree of landscape fragmentation is assessed, assuming a higher degree of habitat separation to result in a higher potential for allopatric speciation. To identify isolated habitat patches within a moving window, TREED employs an image segmentation algorithm. The highest degree of landscape fragmentation is obtained if no grid cell within the considered moving window has a neighbouring grid cell of the same vegetation class (i.e., the number of isolated habitat patches is equal to the number of grid cells). The landscape fragmentation index (LFI) is calculated as:

$$LFI = \frac{\#\ of\ isolated\ habitat\ patches}{\#\ of\ cells\ in\ considered\ window} \tag{62}$$

The potential diversity index (*DI;* dimensionless) of a location is obtained by multiplying the cell-level functional diversity potential with the two derived metrics of landscape-level habitat heterogeneity and fragmentation centred around the grid cell of interest:

$$DI = FDI \cdot LHI \cdot LFI \tag{63}$$

The calculated diversity metrics can only cover the abiotic diversity potential at the level of the climate input resolution and does not resolve sub-grid scale environmental heterogeneity. Accordingly, for comparisons between model runs, only models using the same input resolution can be compared.

4 Comparison to previous model version

The presented TREED version 1.0 is a development from a previous implementation, TREED version 0.1 (Rogger et al., 2025), with major changes regarding model structure, functions and user accessibility. For version 1.0, the model was translated to the Julia language (Bezanson et al., 2017) to enable multithreading and allowing to run simulations at below 1° longitude x 1° latitude resolution at low computational cost. With the current implementation, a global simulation without the calculation of biodiversity metrics at 0.5° longitude and latitude resolution runs in 5 minutes, using 8 threads on a standard desktop computer (Intel(R) Core(TM) Ultra 7 265 (2.40 GHz) processor). At 1°, 2° and 4° resolution, the same simulation is completed in 65, 20, and 7 seconds, respectively.

All functions regarding biodiversity assessment, including the estimations of functional diversity, landscape heterogeneity and landscape fragmentation are new to this version. These functions depend on the model's capacity to resolve high spatial

https://doi.org/10.5194/egusphere-2025-6002
Preprint. Discussion started: 17 December 2025

resolutions, given the importance of landscape-scale topographic and climatic features in determining biodiversity gradients (see section 5.4). The biodiversity metric calculations will allow to use TREED not only for questions related to carbon cycling, but the combined evolution of Earth's carbon cycle and plant biodiversity through time.

Several aspects regarding modelling approach have been changed. This includes the translation of the model from an agent-based model, where plant individuals were tracked in space and time, to a grid-based model, where all operations are run on a per-cell basis (e.g., per cell trait optimization, dispersal as a moving window operation). This increases computational performance by reducing the number of operations per time step, and increases accessibility of the model by simplifying model structure and handling. A major change further includes the simultaneous optimization-based prediction of all plant traits in equilibrium with the environment (eq. 49), enabling a steady state model prediction within one time step. Previously, traits were optimized sequentially, making it necessary to run spin-up simulations and preventing to use the model as a continuous steady state model, which is often required in paleoclimate research. The model now comes with different model run functions, allowing to either conduct a continuous steady state simulation (TREEDsteadycontinuous.jl), a one time step steady state simulation for coupling with other models (TREEDsteadystep.jl), a continuous simulation in eco-evolutionary mode considering dispersal and adaptation (TREEDnonsteadycontinuous.jl), or a one time step simulation in eco-evolutionary mode, allowing to restart the model from a previous time step and enabling the coupling with other models, such as climate or global biogeochemical models. The application of these model functions is illustrated in the case studies presented in the following and that are provided on the code repository.

The new model has been implemented with a focus on user accessibility, making it possible to design model experiments within a few lines of codes and to easily access and modify model parameters (e.g., case studies on code repository). Together with the different model run functions and reduced computational time, these changes make the model particularly suited to quickly set it up for different periods in the geologic past and to run sensitivity tests (e.g., see section 6).

5 Evaluation against present-day observations

5.1 Input and reference data

To evaluate the performance of the TREED model, we run one time step of the model using multi-year monthly average temperature, precipitation, downwelling shortwave radiation and cloud cover data from the years 1981-2010 from CHELSA (Karger et al., 2017) at 0.5° resolution in longitude and latitude. Derived carbon fluxes are evaluated using MODIS-derived GPP and NPP estimates, considering average fluxes from the years 2001-2010 (Kern, 2024). Vegetation height is compared to a combined satellite data and machine-learning based estimate for the year 2010 from Lang et al., (2023). Aboveground and belowground biomass carbon densities are compared to a machine-learning-based upscaling approach from field measurements and satellite data (Huang et al., 2021; Santoro et al., 2010). Evapotranspiration rates are compared to estimates from the Global Land Evaporation Amsterdam Model of the year 2010 (Miralles et al., 2011). Predicted latitudinal gradients

https://doi.org/10.5194/egusphere-2025-6002
Preprint. Discussion started: 17 December 2025

of leaf longevity and leaf mass per area (*LMA = 1/SLA)* are compared to data-based trends derived from the Glopnet data set (Wang et al., 2023; Wright et al., 2004). To evaluate the TREED prediction of potential plant biodiversity at the landscape level, we compare the modelled diversity index to an ensemble prediction of global-scale plant species richness derived from observational records and extrapolation using machine-learning and statistical methods by Cai et al., (2023).

5.2 Evaluation of modelled carbon and water fluxes

The optimality-based prediction of vegetation functioning using the TREED model reasonably approximates the major distribution of photosynthetic carbon assimilation and evapotranspiration (Fig. 4, Fig. 5 a-c). For NPP and GPP, a tendency for an overprediction of carbon assimilation is observed in Indo-Malayan tropical rain forest climates and the subtropics of North and South America. An underestimation is observed in Southeast Asia, tropical savannas and regions of the Mediterranean. Globally, the errors tend to be well balanced with a RMSE of 230 g C m^{-2} for GPP and 113 g C m^{-2} for NPP. The TREED steady-state prediction of the global NPP of 52 Pg C is in good correspondence with an estimated mean global NPP of 56.2 ± 14.3 (± standard deviation) from multiple data- and model-based NPP estimates compiled by Ito (2011).
The model reproduces the global distribution of evapotranspiration, and thus reasonably approximates the carbon-water exchange during photosynthesis. However, there is a tendency for a slight but consistent underprediction of evapotranspiration rates (Fig. 5c), particularly in mid-latitude, temperate regions (Fig. 4 e and f). Given that carbon fluxes are well reproduced in the model, a possible explanation for this mismatch is the lack of an explicit representation of non-photosynthesis related water fluxes, including bare soil evaporation or evaporation of water intercepted on vegetation surfaces.

https://doi.org/10.5194/egusphere-2025-6002
Preprint. Discussion started: 17 December 2025

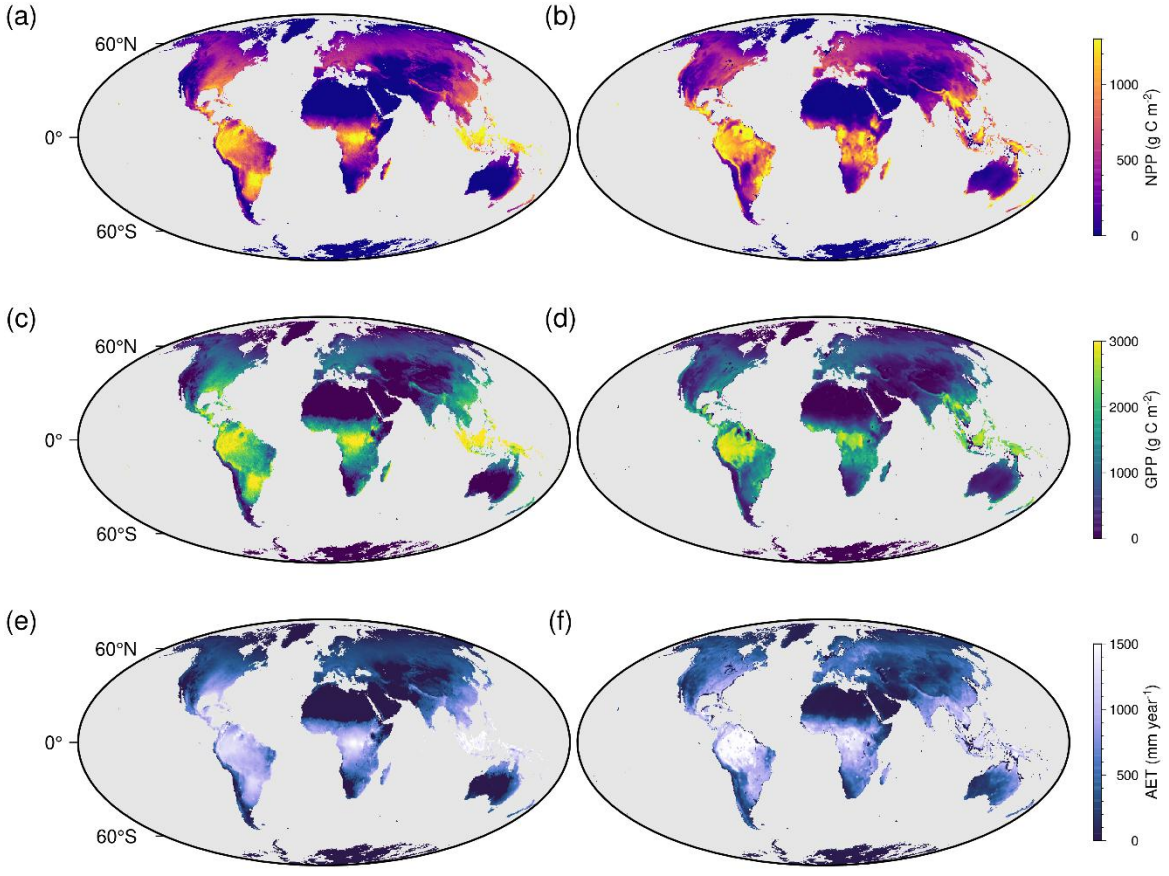

Figure 4: Spatial distribution of modelled and observed carbon and water fluxes. The left column represents model-derived estimates, the right column represents observation-based estimates of (a) & (b) net primary productivity (NPP), (c) & (d) gross primary productivity (GPP), and (e) & (f) evapotranspiration (AET). Carbon flux data from Kern (2024), evapotranspiration from Miralles et al., (2011).

https://doi.org/10.5194/egusphere-2025-6002
Preprint. Discussion started: 17 December 2025

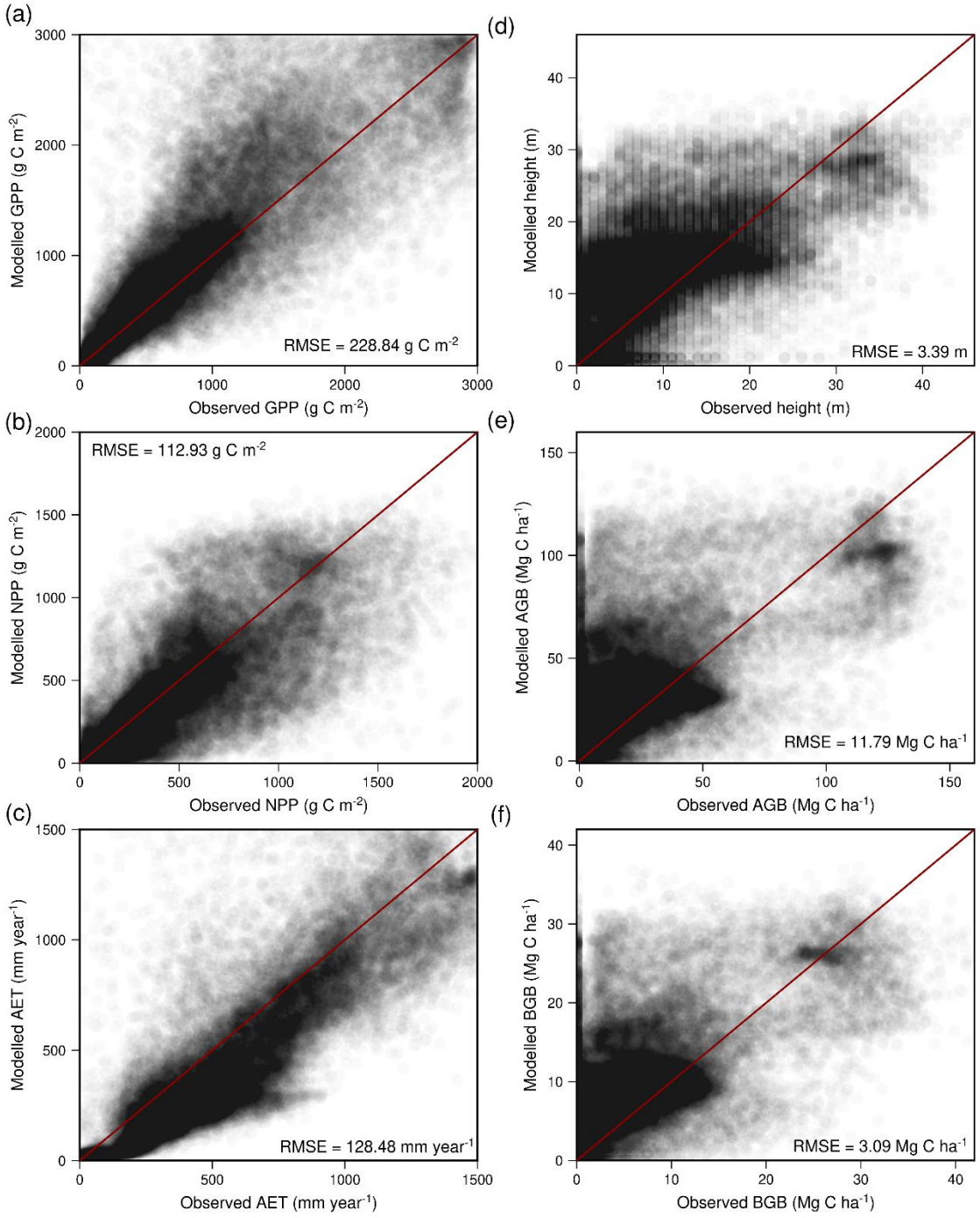

Figure 5: Comparison of modelled and observed carbon and water fluxes (left), and carbon storage (right). (a) Gross primary productivity (GPP), (b), net primary productivity (NPP) and evapotranspiration (AET). (d) Canopy height, (e) above ground biomass carbon storage (AGB), and (f) below ground biomass carbon storage (BGB). The 1:1 line is indicated in red.

https://doi.org/10.5194/egusphere-2025-6002
Preprint. Discussion started: 17 December 2025

RMSE is the root mean square error. Carbon fluxes from Kern (2024), evapotranspiration from Miralles et al. (2011), height data from Lang et al. (2023), biomass data from Huang et al. (2021) and Santoro et al. (2010).

5.3 Evaluation of modelled vegetation height, biomass, leaf characteristics and phenology

The TREED model allows a reasonable approximation of the first-order distribution of vegetation height and biomass (Fig. 6, Fig. 5 d-f). For vegetation height, the model generally results in an overly smooth height distribution and an overprediction in some regions compared to the data for the year 2020. Several reasons may contribute to the overprediction of height, while GPP and NPP errors tend to be better balanced. In the model's height optimization, a surplus NPP will result in a prediction of increased height and biomass growth, until respiratory and tissue turnover carbon investments exceed the surplus carbon from photosynthesis. Compared to the data, there is a space in the height to NPP distribution that is currently not covered by the model (Fig. 7 a). Reduced height growth under high NPP levels indicates carbon turnover processes that are not currently represented in TREED and its height optimization. Some environments may be associated with increased carbon investments for tissue turnover due to disturbances, including fires or harsh environmental conditions such as heat or cold conditions, which could reduce the longevity of vegetation structures. A reduced availability of carbon for height growth may also represent increased carbon investments into biotic interactions, including defence and competition mechanisms other than height growth for light resources. Further, reduced height growth may be a result of additional carbon allocation trade-offs, for example carbon costs associated with hydraulic tissues that scale with plant height but that are not included in the model. Finally, in the height comparison it should also be noted that the model does not consider a present-day land-use map and human influences, and no herbivory.

There is a strong relationship between vegetation height and biomass carbon storage, which is reproduced in the calibration of allometric constants in the model (Fig. 7 b), and drives the modelled spatial distribution of aboveground and belowground biomass (Fig. 6 c-f). Due to the strong biomass to height relationship, mismatches between modelled and observed belowground- and aboveground biomass primarily occur in regions where there is a mismatch in the height prediction.

https://doi.org/10.5194/egusphere-2025-6002
Preprint. Discussion started: 17 December 2025

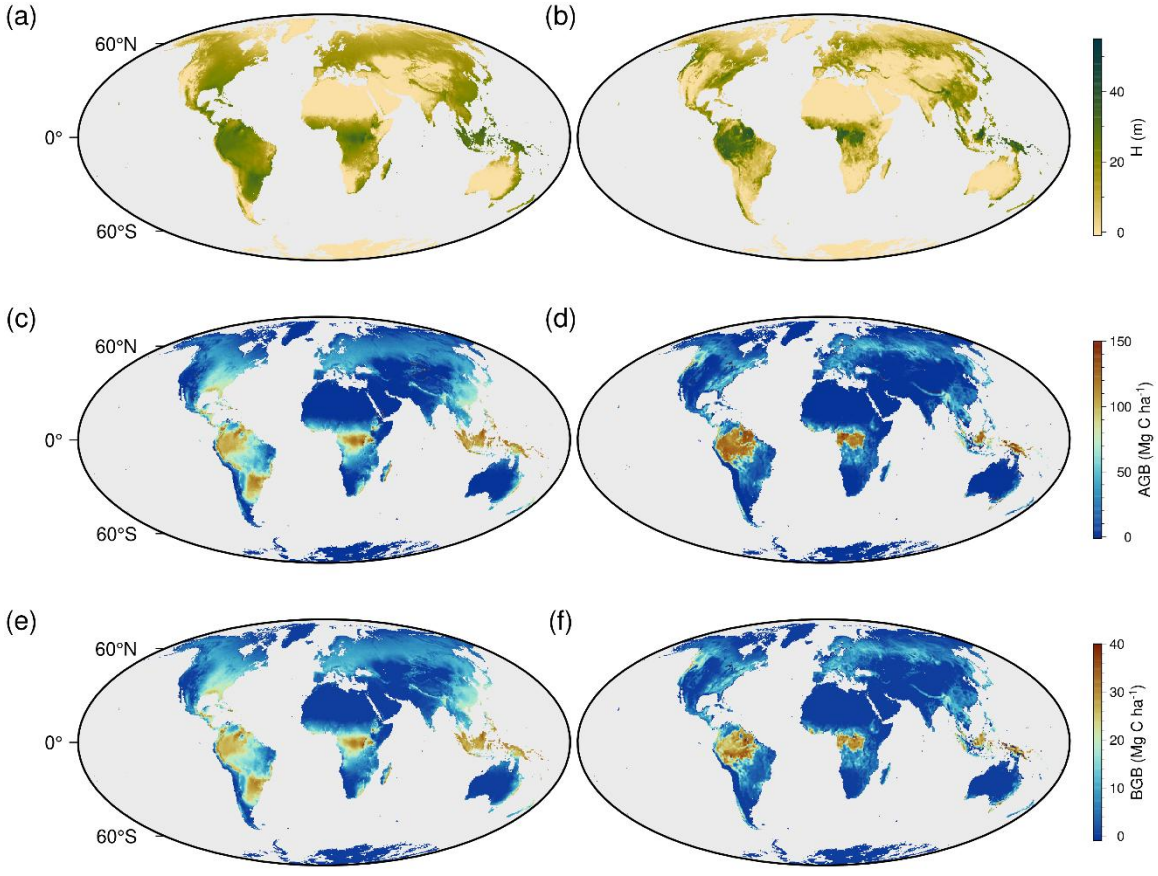

Figure 6: Spatial distribution of modelled and observed vegetation structure and carbon sequestration. The left column represents model-derived estimates, the right column represents observation-based estimates of (a) & (b) vegetation height (c) & (d) above ground biomass (AGB), and (e) & (f) below ground biomass (BGB). Height data from Lang et al. (2023), biomass data from Huang et al. (2021) and Santoro et al. (2010).

https://doi.org/10.5194/egusphere-2025-6002
Preprint. Discussion started: 17 December 2025

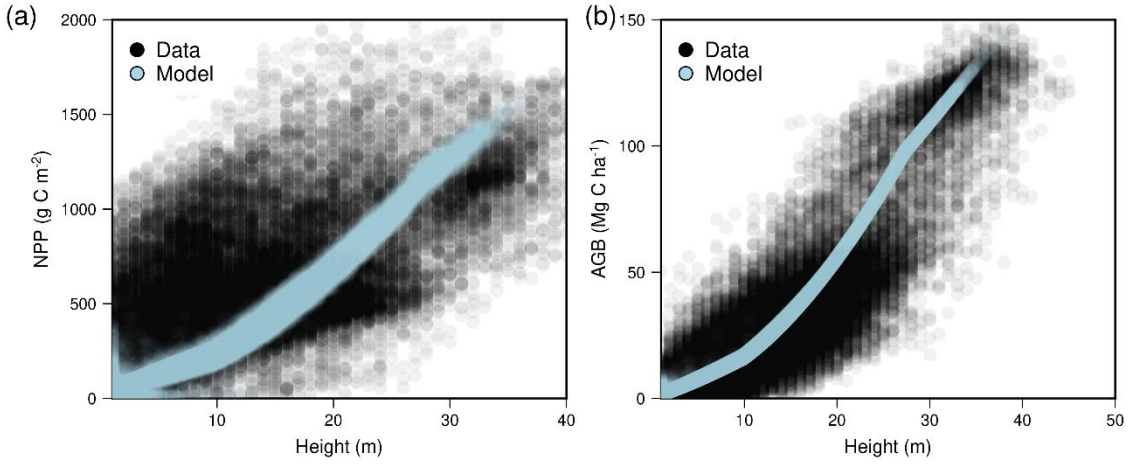

Figure 7: Relationship between vegetation height and carbon fluxes observed in the TREED model and data. (a) Relationship between local rates of net primary productivity (NPP) and height. The model captures the first-order relationship between height and NPP but does not well resolve high NPP/low height combinations, likely associated with carbon turnover processes not currently represented. (b) The modelled biomass distribution across the globe is driven by the strong association between vegetation height and biomass storage. Carbon fluxes from Kern (2024), height data from Lang et al. (2023), biomass data from Huang et al. (2021) and Santoro et al. (2010).

The TREED prediction of deciduous vegetation phenology agrees with the present-day distribution of temperate deciduous broad-leaved forests, with highest frequencies of such growth forms in East Asia, Europe and eastern North America (Fig. 8). Together with the tropics, these regions are associated with predicted leaf longevities of around a year or less. Persistent leaves with longevities of longer than two years are primarily observed in arid or cold regions with a limited growing season length. In line with the carbon economics spectrum (Wright et al., 2004), this tendency indicates a more conservative leaf strategy with lower annual leaf building costs and light acquisition potential but longer persistence. The model captures the major latitudinal patterns of leaf longevity and leaf mass per area (*LMA = 1/SLA*) on the globe, with increasing *LMA* and leaf longevities for evergreen plants, and a decreasing latitudinal trend observed for deciduous plants (Kikuzawa et al., 2013; Reich et al., 2014; Wang et al., 2023). Latitudinal variations are driven by the availability of light, colder temperatures towards the poles and therefore, decreasing growing season lengths. Deciduous and evergreen plants follow contrasting strategies to adjust to these environmental changes (Wang et al., 2023), which are captured by the model and its optimality-based trait prediction. For deciduous plants, shorter growing season are associated with reduced leaf longevities. To compensate a reduction in the carbon sequestration potential due to the shortened growing season length, deciduous plants require more acquisitive leaf structures and a reduced *LMA*. Evergreen plants, on the other hand, compensate the shorter growing seasons, reduced light, and colder temperatures by reducing annual carbon investments into leaves, increased *LMA* and longer persistence.

https://doi.org/10.5194/egusphere-2025-6002
Preprint. Discussion started: 17 December 2025

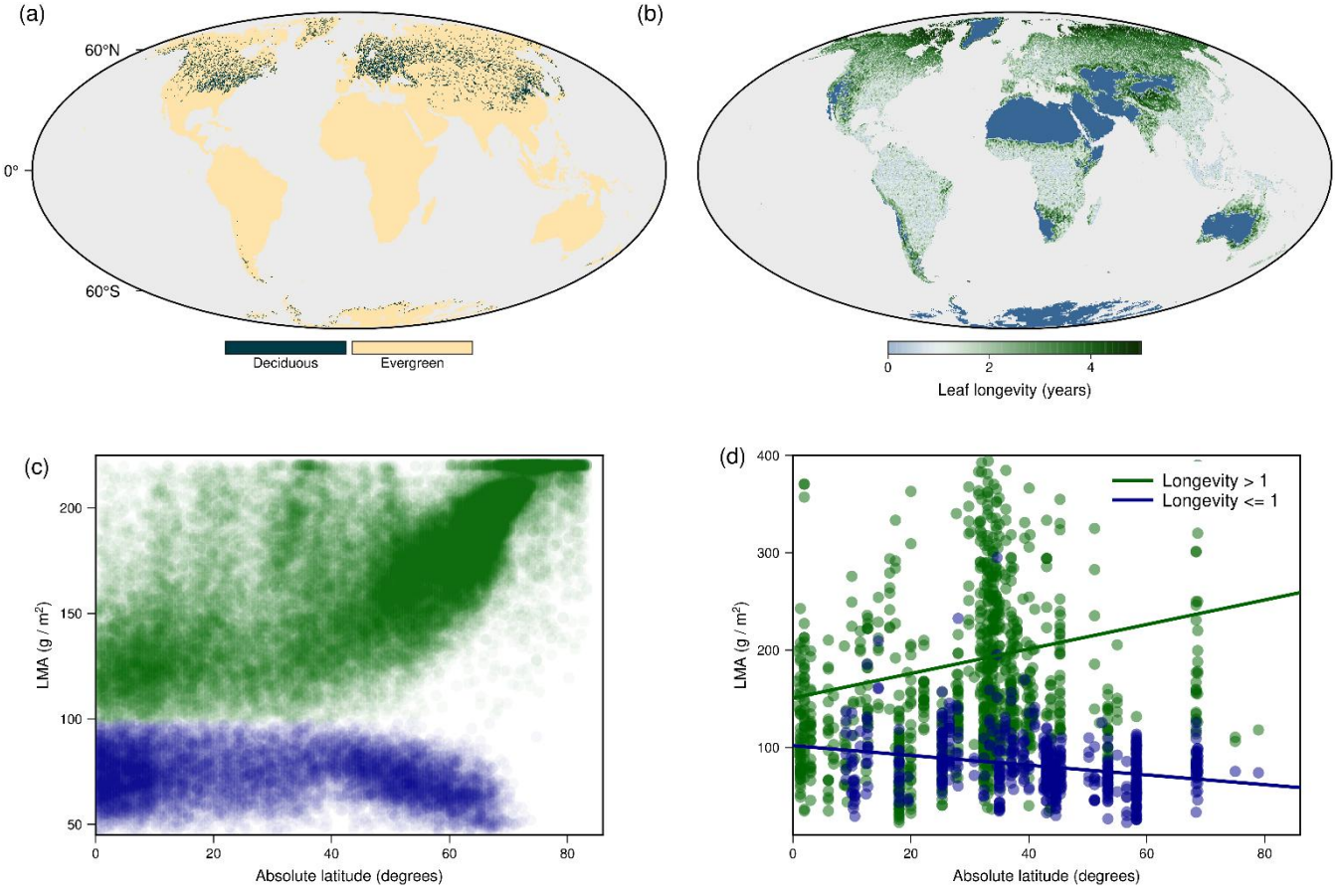

Figure 8: Modelled vegetation phenology and leaf characteristics. (a) Distribution of deciduous or evergreen vegetation units. (b) Modelled average leaf lifespan. (c) Latitudinal distribution of leaf longevity and leaf mass per area (LMA). (d) Observed latitudinal distribution of LMA for evergreen (longevity > 1 year) and plants having leaf life cycle durations of less than a year (longevity ≤ 1 year), data from the Glopnet data set (Wang et al., 2023; Wright et al., 2004).

5.4 Evaluation of modelled plant diversity potential

The diversity calculations in TREED capture a large degree of the observed global plant species diversity distribution (Fig. 9), with an underprediction of the species richness in hotspot regions. The diversity potential in TREED is a compound product of three indices: a functional richness index (*FDI*), a landscape heterogeneity index (*LHI*) and a landscape fragmentation index (*LFI*) (see eq. 63). The functional diversity index (Fig. 9 a) strongly resembles the global pattern of vegetation height and carbon assimilation, indicating that it is primarily a function of the resource availability. In the model, locations with high levels of radiation and water, together with suitable temperatures for photosynthesis, result in a larger range of growth forms and trait combinations that can be sustained and potentially co-exist. The two indices of landscape complexity (*LHI* and *LFI*) capture regions of high topographic complexity, including the Andes, Himalayas, the east African mountains and the Alps.

https://doi.org/10.5194/egusphere-2025-6002
Preprint. Discussion started: 17 December 2025

Topographic complexity in these regions results in a high variability of climatic conditions and thus vegetation habitats. Further, in topographically complex regions the arrangement of vegetation habitats shows a higher degree of fragmentation, which may be associated with dispersal barriers that promote allopatric speciation processes (i.e., speciation by isolation). Combining functional diversity as an indicator of the local diversity potential and the two landscape metrices effectively captures major biodiversity gradients on Earth, with a spearman ranked correlation between the modelled diversity index and observed species richness of 0.81. A major underestimation of the diversity potential is observed in South-East Asia, likely driven by an underestimation of the productivity potential in the region (Fig 4 a-b) and thus a reduced functional diversity potential. Similarly, an overprediction of diversity is observed in the central African tropics, likely related to an overprediction of the productivity and functional diversity potential in the region.

https://doi.org/10.5194/egusphere-2025-6002
Preprint. Discussion started: 17 December 2025

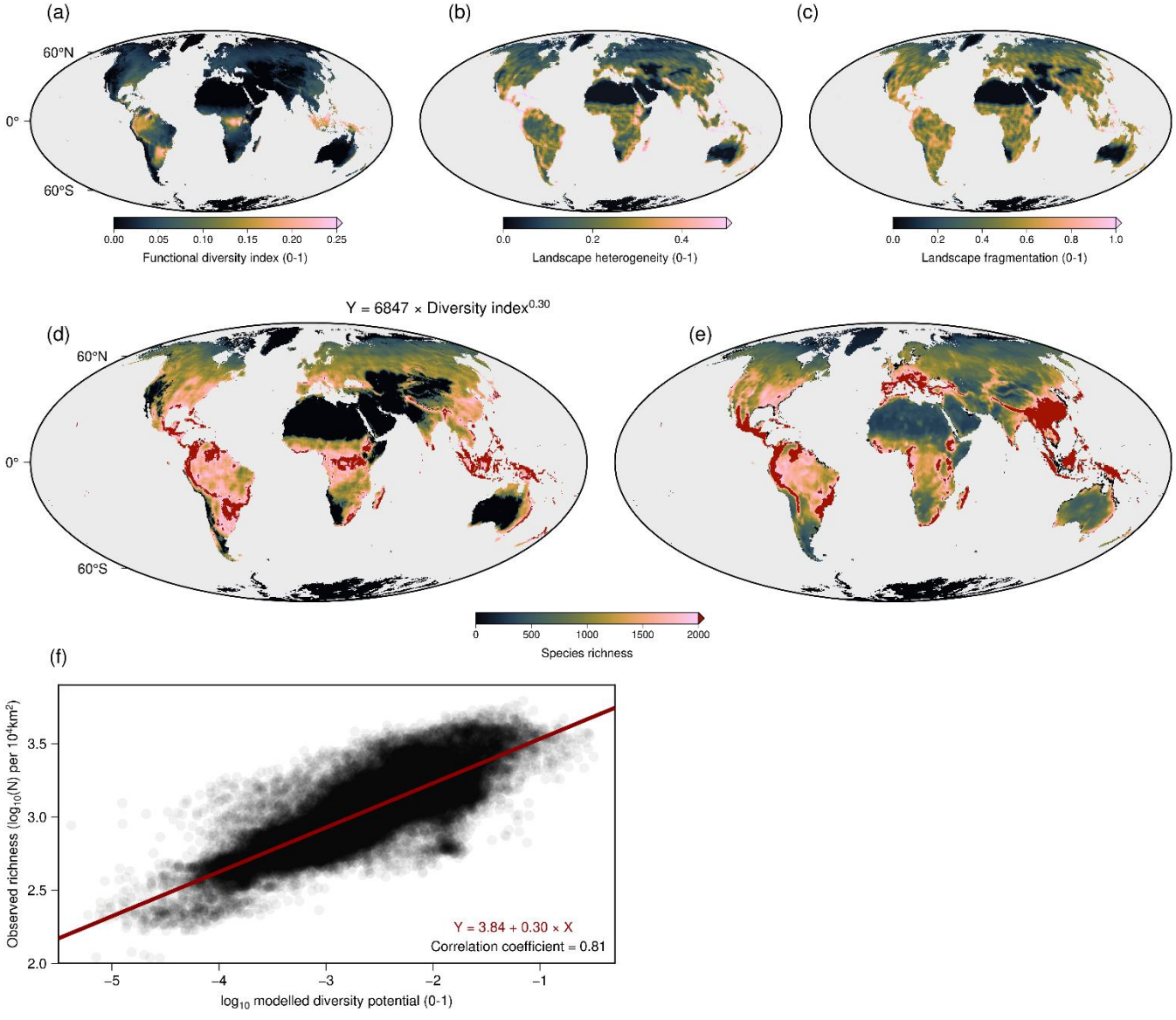

Figure 9: Comparison of modelled plant biodiversity potential and observed species richness data. (a) TREED functional diversity index, (b) landscape heterogeneity index, (c) landscape fragmentation index. Together (a)-(c) represent the components of the diversity index. (d) Predicted species richness using a power law fit between observed species richness and the calculated diversity index (derived by multiplication of functional diversity, landscape heterogeneity and fragmentation indices). (e) Observed plant species richness from Cai et al. (2023). Species richness in (d) and (e) is given as number of species per 10'000 km^2. (f) log-log relationship between modelled diversity potential and observed richness.

https://doi.org/10.5194/egusphere-2025-6002
Preprint. Discussion started: 17 December 2025

6 Paleo-application and eco-evolutionary mode

With regards to computational demand, necessary climatic inputs and model complexity, the TREED model is designed to study vegetation, climate and carbon cycle dynamics over geologic time. The model can either be used to obtain a continuous steady-state prediction of vegetation functioning, structure and diversity, or to study eco-evolutionary transitions of vegetation during periods of environmental change. To illustrate the latter functionality, we apply the model to the Paleocene-Eocene Thermal Maximum (PETM). The PETM was a 5-6 °C global warming event that was triggered by a geologically abrupt release of several thousand Pg of carbon into Earth's atmosphere and oceans (Harper et al., 2024). The climatic perturbation resulted in major shifts in the vegetation distribution and carbon sequestration potential (Bowen, 2013; Bowen and Zachos, 2010; Korasidis et al., 2022). A loss and a 70-100 kyr lagged regrowth of biospheric carbon stocks was suggested to have been a primary driver for the long duration and timing the termination of the PETM warming event (Bowen, 2013; Bowen and Zachos, 2010). A perturbation and loss of vegetation-mediated carbon and climate regulation has also been suggested to have driven the severity and duration of other hyperthermal events in Earth's past (Payne et al., 2004; Rogger et al., 2024; Xu et al., 2022, 2025). The TREED model can be used to study global carbon cycle dynamics during such hyperthermal events. Thereby, the model not only produces different carbon sequestration trajectories, but it also tracks the spatial distribution of vegetation traits through time. The trait and carbon flux outputs of TREED can be used in combination with paleobotanical and geochemical records to better understand and constraint the response capacity of vegetation systems to large-scale carbon cycle perturbations in Earth's past (Rogger et al., 2025).

In the following, we force the TREED model with PETM climate model simulation data from Korasidis et al., (2022) to approximate the changes in vegetation-mediated carbon cycling across the climatic perturbation. For five time steps, the TREED model is forced with pre-PETM climatic conditions at an atmospheric CO_2 level of 680 ppm, followed by a step change to 1590 ppm which is maintained for another 15 model time steps. We keep the notion of "time steps" rather than actual time units in the following, to emphasize that such numerical experiments could be applied to any model duration from centuries to millions of years with the rates of evolution and dispersal being adjusted by the user accordingly.

In Figure 10 a) – d), we show the steady state vegetation height and primary productivity for pre-PETM and peak-PETM CO_2 concentrations. Comparing the two climate states, the model suggests a decreased productivity and vegetation height in tropical and subtropical areas, driven by extreme heat conditions and reduced water availability. In mid to high latitudes, there is a strong increase in vegetation height and productivity, driven by a CO_2 fertilization effect, a higher water-use efficiency and temperatures closer to the optimum photosynthetic temperature between 25 and 30°C (see Eqs. 18-20). Despite the reduced productivity potential in some tropical and subtropical regions, the total global productivity potential increases from around 85 Pg C NPP per year to around 100 Pg C NPP per year.

https://doi.org/10.5194/egusphere-2025-6002
Preprint. Discussion started: 17 December 2025

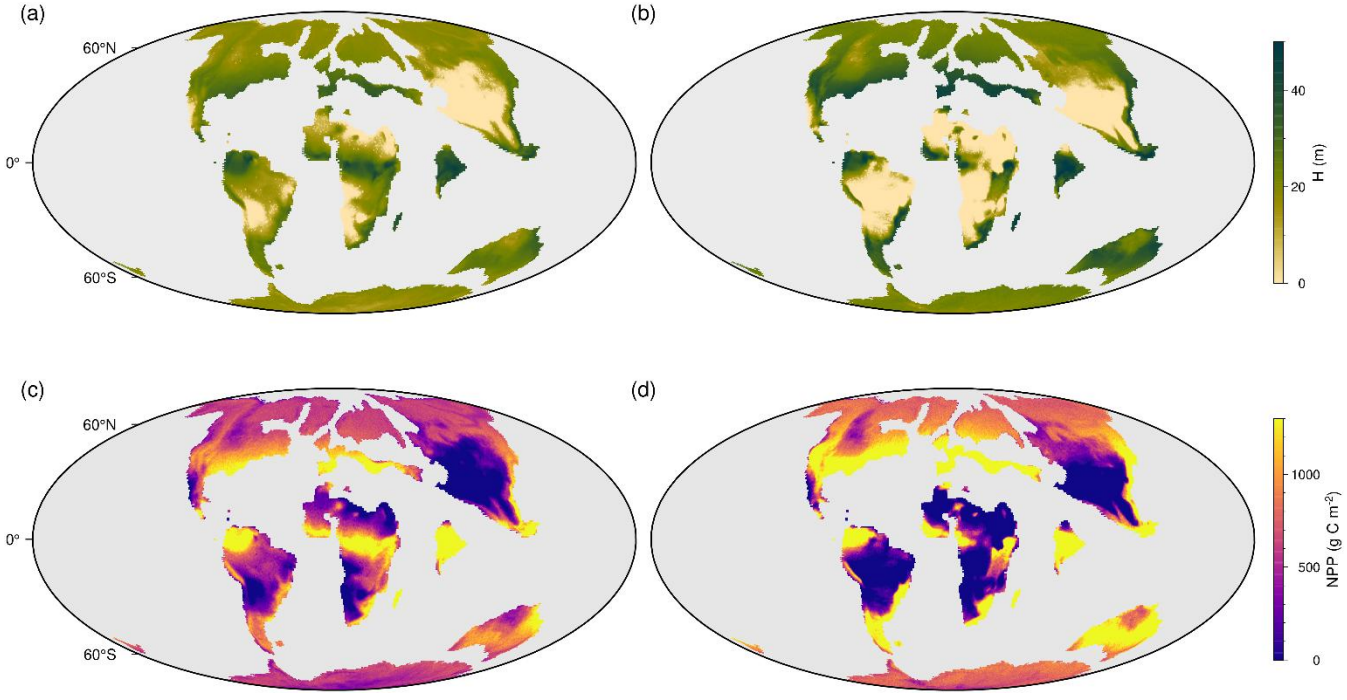

Figure 10: TREED simulation of the PETM. (a) Pre-PETM vegetation height and (c) net primary productivity (NPP) at an atmospheric CO_2 of 680 ppm. (b) PETM vegetation height and (d) net primary productivity at a peak-PETM CO_2 concentration of 1590 ppm.

Whether and how fast the vegetation can capitalize on the globally more optimal productivity conditions strongly depends on the speed of eco-evolutionary adaptation processes and the susceptibility to temperature changes across the transition (Fig. 11). We test a large range of different adaptation scenarios, which is one of the main advantages of the TREED model, and show that the potential of carbon sequestration across a PETM-like climate transitions strongly depends on the biological capacity to adapt to the environmental changes. The observed range of carbon sequestration trajectories, illustrated using the total annual NPP, can be categorized in three potential outcomes illustrated in Fig 11 a. In a scenario where the evolutionary rate of functional and climatic trait adaptation is low (e.g., $\alpha = 0.01$), we observe a strong reduction in the productivity potential due to a loss of adaptation of vegetation to the abruptly changing environmental conditions. Only with time, due to continuous dispersal (e.g., dispersal window radius = 600 km) and slow adaptive evolution, the global productivity potential recovers to levels as during pre-PETM conditions. Due to a low evolutionary adaptation potential, no capitalization of the theoretically possible increase in vegetation productivity is observed until the end of the simulation. Under a scenario of fast trait evolution (e.g., $\alpha = 0.75$), only a limited adaptation and productivity lag following the climatic transition is observed. Due to an efficient adaptation of functional and climatic traits, the vegetation can rapidly capitalize on the climatic conditions in favour of increased primary productivity. A reduced dispersal capacity (e.g., dispersal window radius = 200 km) does not strongly affect

https://doi.org/10.5194/egusphere-2025-6002
Preprint. Discussion started: 17 December 2025

or offset the comparably fast increase in the global productivity potential. If both evolution and dispersal capacity are kept at an intermediate level (e.g., α = 0.1, dispersal window radius = 400 km), an intermediate productivity trajectory is observed. This includes a stress period with a strong reduction of the productivity potential, followed by a recovery and increase of productivity to above pre-PETM levels.

Considering the traits currently included in the TREED model, the capacity of vegetation to endure temperature regimes outside of the original habitat and the capacity to adapt thermal tolerances is found to be the strongest limitation of the global productivity potential (Fig. 11 b). When considering no limitation of productivity due to temperature deviations between the local environment and the climatic environment from which the occupying vegetation originates ($k_{nichebreadth}$ = 0), but considering a low evolutionary rate for other functional traits (a_{ll}, C_{leaf}, and derived H), we do not observe a drop in vegetation productivity. This is because there is no direct stress effect of temperature on productivity, and further, because if plants are not bound to certain climatic environments, there is an unlimited dispersal-based trait exchange. This would for example mean that tropical trees and associated vegetation traits could migrate into temperate conditions without experiencing any physiological stress. If we assume that plant dispersal and trait evolution is bound to certain thermal limits ($k_{nichebreadth}$ > 0), which themselves are subject to evolutionary adaptation, we observe a temporary drop in productivity because there exist climatic environments with no suiting vegetation immediately available, and because dispersal-based trait exchange only occurs within climatic boundaries. In the default eco-evolutionary model, we assume that plant and trait exchange are bound to thermal limits. With a niche breadth parameter $k_{nichebreadth}$ of 0.02, the default model assumes that plants can be productive in environments with deviation in the annual average temperature, the coldest month average temperature, and the warmest month average temperature from their original habitat of up to 15°C. This corresponds approximately to the range temperature variability observed within present-day biomes, which are observed bioclimatic zones of similar vegetation types and characteristics on the globe. Thereby we assume that there exist plant physiological traits, ecosystem characteristics (e.g., competition, herbivory, pests, etc.) or abiotic conditions (e.g., soils and nutrient availability) which limit vegetation exchange to within such climatic boundaries. With every grid cell of the model being initialized with a climatically optimally adapted vegetation, thermal tolerances start to play a role for productivity if the speed of climatic shifts exceed the dispersal capacity of vegetation (Fig. 11 c), and if changes in the temperature distribution exceed the variability observed in the starting climate state. Consequently, we observe a threshold behaviour in the productivity response if we run the model for different land surface warming scenarios across the PETM (Fig. 11 d). For a land surface warming below 4°C and under consideration of limited temperature tolerances ($k_{nichebreadth}$=0.02), no productivity loss is observed. For these warming scenarios, there is an effective dispersal-based vegetation redistribution, and climatic conditions allow for an increased global productivity. For land surface warming scenarios of 6°C or more, a drop and lagged productivity recovery is observed because the speed of climatic change starts to exceed the dispersal-based trait redistribution, and because climatic extremes start to exceed those previously observed. While continuous dispersal-based trait redistribution acts to close the adaptive gap, vegetation is limited by the capacity of adjusting thermal tolerances through acclimation or evolutionary adaptation.

https://doi.org/10.5194/egusphere-2025-6002
Preprint. Discussion started: 17 December 2025

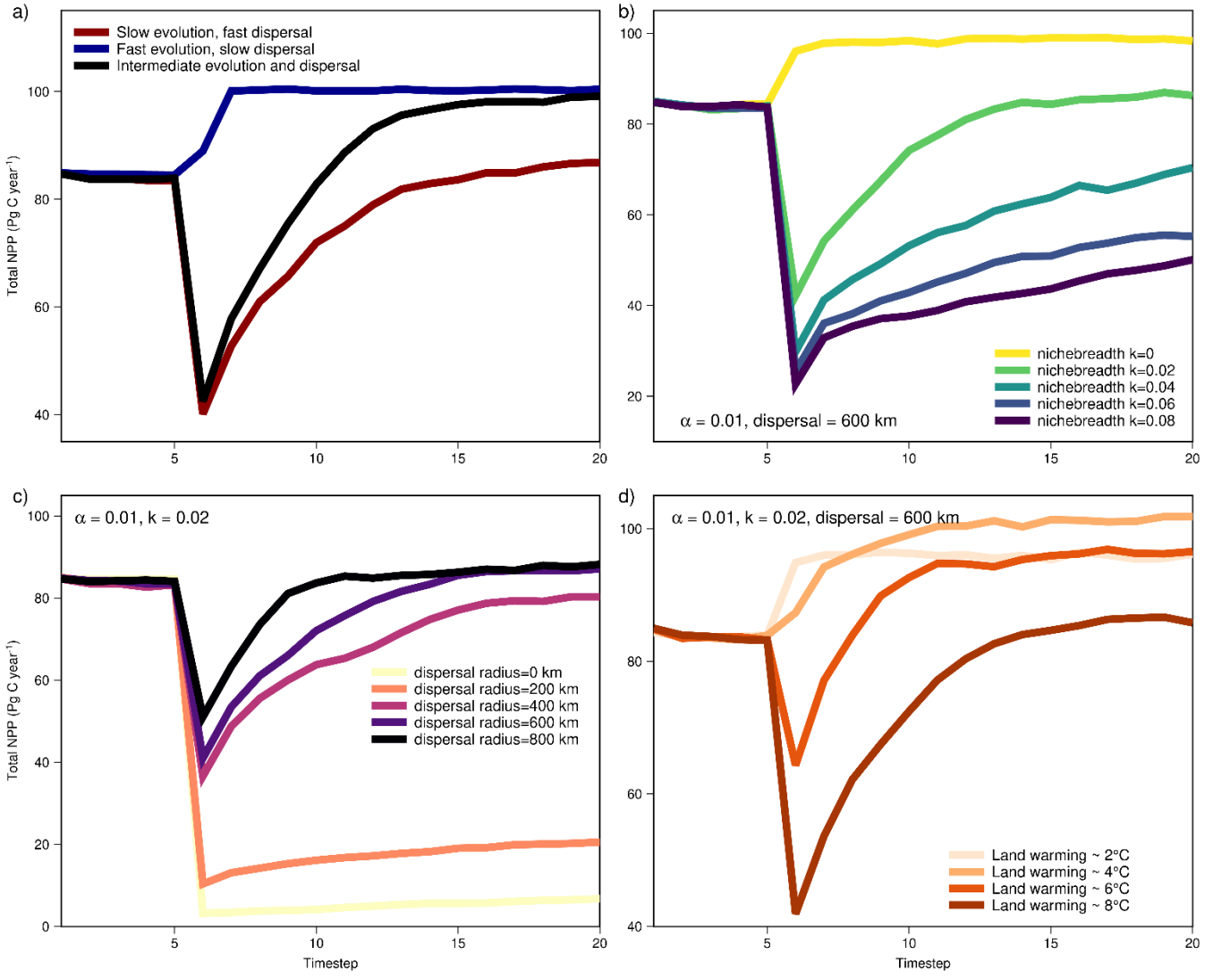

755 **Figure 11: Simulated net primary productivity (NPP) trajectories across the PETM.** Simulated NPP trajectories assuming (a) different adaptation and dispersal rates, (b) different climate niche breadths (*k*) and thermal tolerances, (c) different dispersal rates, and (d) different land surface warming scenarios.

7 Discussion

Using a generalized plant physiology and optimality principles, the TREED model approximates the functioning and structure
760 of present-day vegetation systems, including carbon and water fluxes, height, biomass carbon storage, leaf characteristics, phenology as well as the global distribution of plant species diversity. The model treats trait evolution as an optimization problem under consideration of carbon allocation trade-offs in a continuous trait space, thereby avoiding the use of discrete,

https://doi.org/10.5194/egusphere-2025-6002
Preprint. Discussion started: 17 December 2025

pre-parametrized vegetation classes. Our results support the use of organizing principles of biological systems, such as natural selection, to obtain more self-consistent and parameter-scarce mechanistic models of vegetation dynamics under variable climatic conditions, offering new ways to explore the interactions between vegetation dynamics and climatic variation across timescales from the deep past to the present.

7.1 Evaluation of modelled carbon dynamics and traits

Plant carbon and water exchange, as well as biomass carbon storage, represent major forcings in Earth's carbon and climate system. The TREED model can serve as a computationally efficient, first-order approximation of the large-scale patterns of carbon assimilation and sequestration at present and under different planetary climate states in the past and future. Thereby, the model uses comparatively little input data of monthly average temperature, radiation, precipitation and cloud cover. Global trends in carbon and water fluxes (i.e., GPP, NPP, AET) are predicted with more confidence than vegetation biomass carbon sequestration. The performance difference between carbon fluxes and storage indicates that the optimization procedure is well suited to capture the carbon assimilation potential under given climatic conditions but does not resolve the full variability of how the assimilated carbon is invested into growth and biomass. A discrepancy in the performance of models to predict productivity compared to biomass storage is a feature observed across many vegetation models and is partly explained by the difficulty to resolve carbon turnover times of biomass (Pugh et al., 2020). In the TREED model, the largest biomass carbon pools (heartwood, sapwood, coarse root) are associated with fixed turnover times in the range observed and modelled for the present day (Pugh et al., 2020), while functional relationships determine fine root and leave carbon turnover. In natural systems, turnover of large structural carbon pools is primarily a result of vegetation mortality, driven by a combination of biotic (e.g., competition, herbivory, diseases) and abiotic (e.g., fires, droughts, windthrow) factors (Franklin et al., 1987). A large range of mechanistic formulations exist to approximate these processes, but are associated with considerable uncertainty and differences among models (Pugh et al., 2020). Following other vegetation models (Schaphoff et al., 2018; Sitch et al., 2003), the TREED model further simplifies growth respiration and reproduction carbon costs as fixed fractions of GPP and NPP, respectively. The current implementation of the vegetation carbon turnover and mass balance represents a simple first approximation, with the model being flexible to further develop and test increased complexity formulations of carbon turnover that may depend on environmental conditions or functional trait trade-offs.

In the current TREED version, the considered carbon economic trade-offs and main axes of trait variation include carbon investment into height growth, the leaf carbon pool, leaf longevity and phenology (e.g., Figs. 6 & 8). The underlying allocation dynamics and trade-offs of height growth and leaf carbon economics are well established in both present day vegetation systems (Falster and Westoby, 2003; Valentine and Mäkelä, 2012; Wang et al., 2023; Wright et al., 2004), as well as in the geologic past (McElwain et al., 2024; Soh et al., 2017). With these trade-offs, the model resolves the two main axes of variation in vegetation growth forms observed in plants today (Díaz et al., 2016). However, while capturing mean trends, the model does not resolve the full range of trait variability and complexity we observe in natural vegetation systems. An increase in the modelled trait variability or the range of independent axes of trait variation would require the formulation of additional trait

https://doi.org/10.5194/egusphere-2025-6002
Preprint. Discussion started: 17 December 2025

trade-offs that capture the cost and benefits of growth strategies in given abiotic and biotic environmental conditions. Thereby, the trait trade-off should not be specific to a species or location, but generally applicable across plant species, space and time. The increasing availability of plant functional trait data from various environments at present (Bruelheide et al., 2018; Diaz et al., 2001; Kattge et al., 2020), as well as the geologic past (McElwain et al., 2024), is essential to establish such general trait relationships. The capacity of the TREED model to resolve major patterns in present-day vegetation structure and functioning based on a small number of functional trade-offs illustrates the potential of trait-based models in leading to more generalizable and self-consistent representations of vegetation systems, and may allow a reduction of uncertainty in model-predicted carbon and climate dynamics associated with vegetation parametrizations under environmental conditions of the future (Berzaghi et al., 2020; Fisher et al., 2014) or the deep past (Matthaeus et al., 2023).

7.2 Paleo applications and eco-evolutionary dynamics

Focusing on basic principles of trait functional relationships, a continuous trait space and no pre-parametrized vegetation classes, the TREED model is intended to provide a tool to understand how Earth's climate, topography and vegetation have co-evolved through time. While the fundamental trade-offs of height growth and the leaf economics spectrum that drive the model are expected to also have played out in the distant geologic past (Butrim et al., 2024; Falster and Westoby, 2003; McElwain et al., 2024; Soh et al., 2017), two limitations for the application to the geologic past should be noted. Even though applying a generalized physiology across all plants, the TREED model still takes a present day-derived perspective on traits and whole-plant architecture in the form of the applied allometric and functional relationships. Further, the model assumes a constant theoretically possible trait space for the main varying traits and their combinations. The model does not resolve how the availability of genetic variance may have limited the range of plausible trait combinations through time. The major advantage of TREED with regards to these uncertainties, however, is its capacity to track combined carbon fluxes as well as associated vegetation structures. The model results can thus be compared to combined geochemical records informing about vegetation productivity (Bowen, 2013; Denis et al., 2021), as well as trait structures derived from paleobotanical records (McElwain et al., 2024; Rogger et al., 2025), to assess the validity of currently implemented and future additions of functional trade-offs and allometric relationships.

To study co-evolutionary transitions between the physical environment and vegetation systems, TREED includes eco-evolutionary adaptation processes not currently considered in standard vegetation models, including the capacity of vegetation to adapt to environmental changes through trait evolution and dispersal dynamics (Berzaghi et al., 2020). A limited capacity of vegetation systems to respond to abrupt climatic changes and a loss of vegetation-mediated climate regulation are considered to have strongly shaped global carbon cycle dynamics in the geologic past, and particularly, during episodes of abrupt climatic change (Hull, 2015; Payne et al., 2004; Retallack et al., 1999; Rogger et al., 2024; Xu et al., 2022, 2025). An evaluation of the capacity of vegetation to respond to environmental change is of particular importance considering that the speed of current climate warming may have no precedent in the last 400 million years (Foster et al., 2017). However, our understanding of the plant-climate adaptation process through acclimatization and evolutionary adaptation, the speed, and its limits, remain an active

https://doi.org/10.5194/egusphere-2025-6002
Preprint. Discussion started: 17 December 2025

area of research (Bennett et al., 2021; Jezkova and Wiens, 2016; Liu et al., 2020; Schneider et al., 2025; Stemkovski et al., 2025). By combining trait-enabled model predictions, geochemical and palaeobotanical records from Earth's past, the TREED model was developed to help constrain and test hypotheses about the vegetation response to past climatic changes, the speed and capacity of adaptation, and how adaptation may depend on the starting climate state and atmospheric CO_2, as well as the rate, spatial distribution and magnitude of climate warming. Obtaining an understanding of these dynamics through geologic time will help to better predict the vegetation responses that may emerge under different scenarios of climate change over the next centuries.

7.3 Plant biodiversity dynamics

We show that the generalized plant physiology and continuous trait space of the TREED model cannot only be used to predict vegetation functioning and structure, but also to estimate locations of a high plant diversity potential. Thereby, we combine measures of local scale diversity (i.e., functional diversity potential) and landscape-scale biodiversity metrics (i.e., landscape heterogeneity and fragmentation of vegetation habitats). The employed metrics are aimed to resolve the two predominant drivers of plant species richness on Earth, including the spatial distribution of productivity-limiting resources such as energy and water, and the distribution of topographic complexity, promoting species diversity though niche differentiation and allopatric speciation (Antonelli et al., 2018; Cai et al., 2023; Kreft and Jetz, 2007; Stein et al., 2014). Our results support that the consideration of these biodiversity drivers captures a large degree of the broad-scale plant biodiversity distribution on Earth today. As such, in the context of paleoecological research, the model represents a tool to evaluate how topographic and climatic changes throughout Earth's history may have influenced the global distribution of the plant biodiversity either through alteration of the functional diversity potential or landscape dynamics. In the biodiversity estimation, the TREED model takes a purely environment-driven approach by estimating a diversity index based on the current timestep's abiotic environmental conditions. Individual species and their life histories are not resolved. As the model does not explicitly represent the biological processes that ultimately lead to the realized global biodiversity distribution of a period (e.g., movement, speciation, extinction), the predicted biodiversity indices should be considered indicators of a diversity potential and not a realized diversity.

7.4 Future developments

Future developments of the TREED model will allow the inclusion and testing of additional functional trait trade-offs, which may help to further generalize the model for its application under past and future climatic conditions, and to resolve growth forms not currently represented (e.g., Fig. 7). Targets for development particularly include functional trade-offs concerning carbon investments into hydraulic traits (e.g., maximum stomatal conductance or xylem conductivity), which are important both in determining the response of vegetation systems to environmental conditions as well as in their impact on the coupled global carbon and water cycle (McElwain et al., 2024). Related to water acquisition, also the competition for pre-emptying water resources from competitors may be considered in future model versions, complementing the current light competition

https://doi.org/10.5194/egusphere-2025-6002
Preprint. Discussion started: 17 December 2025

scheme. In drought-prone environments, a competitive advantage in securing water may favour the relative allocation of carbon into belowground biomass at the expense of height and aboveground biomass growth (Cabal et al., 2020), which is not currently resolved in the model that assumes a constant root to shoot carbon ratio. Further, alternative models concerning carbon turnover costs may be employed. Possible schemes include environment-dependent vegetation mortality, such as increased carbon turnover in heat, drought or wind-prone environments (Pugh et al., 2020), or susceptibility to biotic stresses depending on environment conditions and functional trait characteristics, e.g., increased herbivory pressures in high temperature environments and for low LMA leaf traits (Currano et al., 2008, 2010). Finally, it is aimed to include recently developed, optimality-based and parameter-scarce models of the photosynthetic carbon assimilation and evapotranspiration into TREED (Stocker et al., 2020), which is the physiologic process currently relying on most pre-defined parameter inputs (e.g., Table 1) and which will help to differentiate the influence of short timescale acclimatization processes of the photosynthetic pathway from long-term evolutionary trait evolution in response to climatic change (Schneider et al., 2025).

8 Conclusion

The trait- and optimality-based vegetation model TREED resolves major patterns in present-day vegetation structure, functioning and diversity by resolving optimal trait allocation strategies of leaf characteristics and height growth across environments. The capacity to capture major vegetation characteristics based on a limited set of functional trait trade-offs emphasizes the potential of trait- and optimality-based vegetation models to advance the representation of vegetation systems under changing environmental conditions. By considering trade-offs that apply across species, space and time, optimality-based models may help to reduce uncertainty in vegetation-mediated Earth system process under climatic conditions fundamentally different from the present, as during Earth's past or under future warm climates. Moreover, by combining a continuous functional trait space with landscape-scale variability in vegetation habitats, the TREED model may help to advance our understanding of the coupled evolution of vegetation productivity and diversity through time.

Vegetation plays a fundamental role in Earth's carbon and climate system, mediating fluxes of carbon, water and energy. A loss of vegetation functions due to abrupt environmental perturbations may trigger feedback dynamics not currently resolved in vegetation and Earth system models. The TREED model approximates eco-evolutionary adaptation dynamics including limited trait evolution and dispersal dynamics to investigate the response capacity of vegetation systems. In combination with geochemical and paleobotanical data, the trait-enabled model may help to better understand and constrain the resilience of vegetation-mediated Earth system functions in the geologic past, as well as under future climatic changes.

9 Code and data availability

The TREED v1.0 model code is publicly available on github (https://github.com/julrogger/TREED), and the version of the model used to produce the results presented in this study, along with all necessary input and evaluation data, can be accessed

https://doi.org/10.5194/egusphere-2025-6002
Preprint. Discussion started: 17 December 2025

on Zenodo under accession code 17777279 (https://doi.org/10.5281/zenodo.17777279) under the Apache 2.0 license (Rogger, 2025). The model comes with three case studies showcasing the application of the model functions and for reproducing the results presented in this study. Please see the deposited README file for more information on how to install and run the model.

10 Author contributions

JR developed the model, wrote the model code, conducted the presented analyses, and wrote the first version of the manuscript. KG, EBK, WJM, BJM, BDS, TVG and LP contributed to the conceptualization of the model, aspects of model validation and contributed to the writing of the paper. TVG and LP provided funding.

11 Competing interests

The authors declare that they have no conflict of interest.

12 Acknowledgements

This work was supported by Swiss National Science Foundation grants 200021_231594 and 200021_192296.

13 References

Antonelli, A., Kissling, W. D., Flantua, S. G. A., Bermúdez, M. A., Mulch, A., Muellner-Riehl, A. N., Kreft, H., Linder, H. P., Badgley, C., Fjeldså, J., Fritz, S. A., Rahbek, C., Herman, F., Hooghiemstra, H., and Hoorn, C.: Geological and climatic influences on mountain biodiversity, Nature Geosci, 11, 718–725, https://doi.org/10.1038/s41561-018-0236-z, 2018.

Beck, H. E., Zimmermann, N. E., McVicar, T. R., Vergopolan, N., Berg, A., and Wood, E. F.: Present and future Köppen-Geiger climate classification maps at 1-km resolution, Sci Data, 5, 180214, https://doi.org/10.1038/sdata.2018.214, 2018.

Beerling, D. J. and Berner, R. A.: Feedbacks and the coevolution of plants and atmospheric CO2, Proceedings of the National Academy of Sciences, 102, 1302–1305, https://doi.org/10.1073/pnas.0408724102, 2005.

Bennett, J. M., Sunday, J., Calosi, P., Villalobos, F., Martínez, B., Molina-Venegas, R., Araújo, M. B., Algar, A. C., Clusella-Trullas, S., Hawkins, B. A., Keith, S. A., Kühn, I., Rahbek, C., Rodríguez, L., Singer, A., Morales-Castilla, I., and Olalla-Tárraga, M. Á.: The evolution of critical thermal limits of life on Earth, Nat Commun, 12, 1198, https://doi.org/10.1038/s41467-021-21263-8, 2021.

Berner, R. A.: The phanerozoic carbon cycle: CO2 and O2, Oxford University Press, Oxford, New York, 150 pp., 2004.

https://doi.org/10.5194/egusphere-2025-6002
Preprint. Discussion started: 17 December 2025

Berzaghi, F., Wright, I. J., Kramer, K., Oddou-Muratorio, S., Bohn, F. J., Reyer, C. P. O., Sabaté, S., Sanders, T. G. M., and Hartig, F.: Towards a New Generation of Trait-Flexible Vegetation Models, Trends in Ecology & Evolution, 35, 191–205, https://doi.org/10.1016/j.tree.2019.11.006, 2020.

Bezanson, J., Edelman, A., Karpinski, S., and Shah, V. B.: Julia: A Fresh Approach to Numerical Computing, SIAM Rev., 59, 65–98, https://doi.org/10.1137/141000671, 2017.

Bowen, G. J.: Up in smoke: A role for organic carbon feedbacks in Paleogene hyperthermals, Global and Planetary Change, 109, 18–29, https://doi.org/10.1016/j.gloplacha.2013.07.001, 2013.

Bowen, G. J. and Zachos, J. C.: Rapid carbon sequestration at the termination of the Palaeocene–Eocene Thermal Maximum, Nature Geosci, 3, 866–869, https://doi.org/10.1038/ngeo1014, 2010.

Boyce, C. K. and Lee, J.-E.: Plant Evolution and Climate Over Geological Timescales, Annu. Rev. Earth Planet. Sci., 45, 61–87, https://doi.org/10.1146/annurev-earth-063016-015629, 2017.

Bruelheide, H., Dengler, J., Purschke, O., Lenoir, J., Jiménez-Alfaro, B., Hennekens, S. M., Botta-Dukát, Z., Chytrý, M., Field, R., Jansen, F., Kattge, J., Pillar, V. D., Schrodt, F., Mahecha, M. D., Peet, R. K., Sandel, B., van Bodegom, P., Altman, J., Alvarez-Dávila, E., Arfin Khan, M. A. S., Attorre, F., Aubin, I., Baraloto, C., Barroso, J. G., Bauters, M., Bergmeier, E., Biurrun, I., Bjorkman, A. D., Blonder, B., Čarni, A., Cayuela, L., Černý, T., Cornelissen, J. H. C., Craven, D., Dainese, M., Derroire, G., De Sanctis, M., Díaz, S., Doležal, J., Farfan-Rios, W., Feldpausch, T. R., Fenton, N. J., Garnier, E., Guerin, G. R., Gutiérrez, A. G., Haider, S., Hattab, T., Henry, G., Hérault, B., Higuchi, P., Hölzel, N., Homeier, J., Jentsch, A., Jürgens, N., Kącki, Z., Karger, D. N., Kessler, M., Kleyer, M., Knollová, I., Korolyuk, A. Y., Kühn, I., Laughlin, D. C., Lens, F., Loos, J., Louault, F., Lyubenova, M. I., Malhi, Y., Marcenò, C., Mencuccini, M., Müller, J. V., Munzinger, J., Myers-Smith, I. H., Neill, D. A., Niinemets, Ü., Orwin, K. H., Ozinga, W. A., Penuelas, J., Pérez-Haase, A., Petřík, P., Phillips, O. L., Pärtel, M., Reich, P. B., Römermann, C., Rodrigues, A. V., Sabatini, F. M., Sardans, J., Schmidt, M., Seidler, G., Silva Espejo, J. E., Silveira, M., Smyth, A., Sporbert, M., Svenning, J.-C., Tang, Z., Thomas, R., Tsiripidis, I., Vassilev, K., Violle, C., Virtanen, R., et al.: Global trait–environment relationships of plant communities, Nat Ecol Evol, 2, 1906–1917, https://doi.org/10.1038/s41559-018-0699-8, 2018.

Brunner, I. and Godbold, D. L.: Tree roots in a changing world, Journal of Forest Research, 12, 78–82, https://doi.org/10.1007/s10310-006-0261-4, 2007.

Butrim, M. J., Lowe, A. J., and Currano, E. D.: Leaf mass per area: An investigation into the application of the ubiquitous functional trait from a paleobotanical perspective, American J of Botany, 111, https://doi.org/10.1002/ajb2.16419, 2024.

Cabal, C., Martínez-García, R., De Castro Aguilar, A., Valladares, F., and Pacala, S. W.: The exploitative segregation of plant roots, Science, 370, 1197–1199, https://doi.org/10.1126/science.aba9877, 2020.

Cai, L., Kreft, H., Taylor, A., Denelle, P., Schrader, J., Essl, F., Van Kleunen, M., Pergl, J., Pyšek, P., Stein, A., Winter, M., Barcelona, J. F., Fuentes, N., Inderjit, Karger, D. N., Kartesz, J., Kuprijanov, A., Nishino, M., Nickrent, D., Nowak, A., Patzelt, A., Pelser, P. B., Singh, P., Wieringa, J. J., and Weigelt, P.: Global models and predictions of plant diversity based on advanced machine learning techniques, New Phytologist, 237, 1432–1445, https://doi.org/10.1111/nph.18533, 2023.

https://doi.org/10.5194/egusphere-2025-6002
Preprint. Discussion started: 17 December 2025

Collatz, G. J., Ball, J. T., Grivet, C., and Berry, J. A.: Physiological and environmental regulation of stomatal conductance, photosynthesis and transpiration: a model that includes a laminar boundary layer, Agricultural and Forest Meteorology, 54, 107–136, https://doi.org/10.1016/0168-1923(91)90002-8, 1991.

Currano, E. D., Wilf, P., Wing, S. L., Labandeira, C. C., Lovelock, E. C., and Royer, D. L.: Sharply increased insect herbivory during the Paleocene–Eocene Thermal Maximum, Proc. Natl. Acad. Sci. U.S.A., 105, 1960–1964, https://doi.org/10.1073/pnas.0708646105, 2008.

Currano, E. D., Labandeira, C. C., and Wilf, P.: Fossil insect folivory tracks paleotemperature for six million years, Ecological Monographs, 80, 2010.

Dahl, T. W. and Arens, S. K. M.: The impacts of land plant evolution on Earth's climate and oxygenation state – An interdisciplinary review, Chemical Geology, 547, 119665, https://doi.org/10.1016/j.chemgeo.2020.119665, 2020.

Denis, E. H., Maibauer, B. J., Bowen, G. J., Jardine, P. E., Harrington, G. J., Baczynski, A. A., McInerney, F. A., Collinson, M. E., Belcher, C. M., Wing, S. L., and Freeman, K. H.: Decreased soil carbon in a warming world: Degraded pyrogenic carbon during the Paleocene-Eocene Thermal Maximum, Bighorn Basin, Wyoming, Earth and Planetary Science Letters, 566, 116970, https://doi.org/10.1016/j.epsl.2021.116970, 2021.

Diaz, S., Cabido, M., and Casanoves, F.: Functional implications of trait-environment linkages in plant communities., in: Ecological assembly rules - perspecitves, advances, retreats, edited by: Weiher, E. and Keddy, P., Cambridge University Press, Cambridge, UK, 338–362, 2001.

Díaz, S., Kattge, J., Cornelissen, J. H. C., Wright, I. J., Lavorel, S., Dray, S., Reu, B., Kleyer, M., Wirth, C., Colin Prentice, I., Garnier, E., Bönisch, G., Westoby, M., Poorter, H., Reich, P. B., Moles, A. T., Dickie, J., Gillison, A. N., Zanne, A. E., Chave, J., Joseph Wright, S., Sheremet'ev, S. N., Jactel, H., Baraloto, C., Cerabolini, B., Pierce, S., Shipley, B., Kirkup, D., Casanoves, F., Joswig, J. S., Günther, A., Falczuk, V., Rüger, N., Mahecha, M. D., and Gorné, L. D.: The global spectrum of plant form and function, Nature, 529, 167–171, https://doi.org/10.1038/nature16489, 2016.

Etterson, J. R. and Shaw, R. G.: Constraint to Adaptive Evolution in Response to Global Warming, Science, 294, 151–154, https://doi.org/10.1126/science.1063656, 2001.

Falster, D. S. and Westoby, M.: Plant height and evolutionary games, Trends in Ecology & Evolution, 18, 337–343, https://doi.org/10.1016/S0169-5347(03)00061-2, 2003.

Farquhar, G. D. and Caemmerer, S.: Modelling of Photosynthetic Response to Environmental Conditions, in: Physiological Plant Ecology II: Water Relations and Carbon Assimilation, edited by: Lange, O. L., Nobel, P. S., Osmond, C. B., and Ziegler, H., Springer, Berlin, 549–587, 1982.

Farquhar, G. D., Von Caemmerer, S., and Berry, J. A.: A biochemical model of photosynthetic CO2 assimilation in leaves of C3 species, Planta, 149, 78–90, https://doi.org/10.1007/BF00386231, 1980.

Fisher, J. B., Huntzinger, D. N., Schwalm, C. R., and Sitch, S.: Modeling the Terrestrial Biosphere, Annu. Rev. Environ. Resour., 39, 91–123, https://doi.org/10.1146/annurev-environ-012913-093456, 2014.

https://doi.org/10.5194/egusphere-2025-6002
Preprint. Discussion started: 17 December 2025

Foster, G. L., Royer, D. L., and Lunt, D. J.: Future climate forcing potentially without precedent in the last 420 million years, Nat Commun, 8, 14845, https://doi.org/10.1038/ncomms14845, 2017.

Franklin, J. F., Shugart, H. H., and Harmon, M. E.: Tree Death as an Ecological Process, BioScience, 37, 550–556, https://doi.org/10.2307/1310665, 1987.

Franklin, O., Palmroth, S., and Näsholm, T.: How eco-evolutionary principles can guide tree breeding and tree biotechnology for enhanced productivity, Tree Physiology, 34, 1149–1166, https://doi.org/10.1093/treephys/tpu111, 2014.

Franklin, O., Harrison, S. P., Dewar, R., Farrior, C. E., Brännström, Å., Dieckmann, U., Pietsch, S., Falster, D., Cramer, W., Loreau, M., Wang, H., Mäkelä, A., Rebel, K. T., Meron, E., Schymanski, S. J., Rovenskaya, E., Stocker, B. D., Zaehle, S., Manzoni, S., van Oijen, M., Wright, I. J., Ciais, P., van Bodegom, P. M., Peñuelas, J., Hofhansl, F., Terrer, C., Soudzilovskaia, N. A., Midgley, G., and Prentice, I. C.: Organizing principles for vegetation dynamics, Nat. Plants, 6, 444–453, https://doi.org/10.1038/s41477-020-0655-x, 2020.

Gonzalez, P., Neilson, R. P., Lenihan, J. M., and Drapek, R. J.: Global patterns in the vulnerability of ecosystems to vegetation shifts due to climate change, Global Ecology and Biogeography, 19, 755–768, https://doi.org/10.1111/j.1466-8238.2010.00558.x, 2010.

Gurung, K., Field, K. J., Batterman, S. A., Poulton, S. W., and Mills, B. J. W.: Geographic range of plants drives long-term climate change, Nat Commun, 15, 1805, https://doi.org/10.1038/s41467-024-46105-1, 2024.

Harper, D. T., Hönisch, B., Bowen, G. J., Zeebe, R. E., Haynes, L. L., Penman, D. E., and Zachos, J. C.: Long- and short-term coupling of sea surface temperature and atmospheric CO2 during the late Paleocene and early Eocene, Proc. Natl. Acad. Sci. U.S.A., 121, e2318779121, https://doi.org/10.1073/pnas.2318779121, 2024.

Harrison, S. P., Cramer, W., Franklin, O., Prentice, I. C., Wang, H., Brännström, Å., Boer, H., Dieckmann, U., Joshi, J., Keenan, T. F., Lavergne, A., Manzoni, S., Mengoli, G., Morfopoulos, C., Peñuelas, J., Pietsch, S., Rebel, K. T., Ryu, Y., Smith, N. G., Stocker, B. D., and Wright, I. J.: Eco-evolutionary optimality as a means to improve vegetation and land-surface models, New Phytologist, 231, 2125–2141, https://doi.org/10.1111/nph.17558, 2021.

Haxeltine, A. and Prentice, I. C.: A General Model for the Light-Use Efficiency of Primary Production, Functional Ecology, 10, 551, https://doi.org/10.2307/2390165, 1996a.

Haxeltine, A. and Prentice, I. C.: BIOME3: An equilibrium terrestrial biosphere model based on ecophysiological constraints, resource availability, and competition among plant functional types, Global Biogeochem. Cycles, 10, 693–709, https://doi.org/10.1029/96GB02344, 1996b.

Hilton, R. G. and West, A. J.: Mountains, erosion and the carbon cycle, Nat Rev Earth Environ, 1, 284–299, https://doi.org/10.1038/s43017-020-0058-6, 2020.

Huang, S., Titus, S. J., and Wiens, D. P.: Comparison of nonlinear height-diamter functions for major Alberta tree species, Canadian Journal of Forest Research, 22, 1297–1304, https://doi.org/10.1139/x92-172, 1992.

https://doi.org/10.5194/egusphere-2025-6002
Preprint. Discussion started: 17 December 2025

Huang, Y., Ciais, P., Santoro, M., Makowski, D., Chave, J., Schepaschenko, D., Abramoff, R. Z., Goll, D. S., Yang, H., Chen, Y., Wei, W., and Piao, S.: A global map of root biomass across the world's forests, Earth Syst. Sci. Data, 13, 4263–4274, https://doi.org/10.5194/essd-13-4263-2021, 2021.

Hull, P.: Life in the Aftermath of Mass Extinctions, Current Biology, 25, R941–R952, https://doi.org/10.1016/j.cub.2015.08.053, 2015.

Ito, A.: A historical meta-analysis of global terrestrial net primary productivity: are estimates converging?, Global Change Biology, 17, 3161–3175, https://doi.org/10.1111/j.1365-2486.2011.02450.x, 2011.

Jezkova, T. and Wiens, J. J.: Rates of change in climatic niches in plant and animal populations are much slower than projected climate change, Proc. R. Soc. B., 283, 20162104, https://doi.org/10.1098/rspb.2016.2104, 2016.

Judd, E. J., Tierney, J. E., Lunt, D. J., Montañez, I. P., Huber, B. T., Wing, S. L., and Valdes, P. J.: A 485-million-year history of Earth's surface temperature, Science, 385, eadk3705, https://doi.org/10.1126/science.adk3705, 2024.

Karger, D. N., Conrad, O., Böhner, J., Kawohl, T., Kreft, H., Soria-Auza, R. W., Zimmermann, N. E., Linder, H. P., and Kessler, M.: Climatologies at high resolution for the earth's land surface areas, Sci Data, 4, 170122, https://doi.org/10.1038/sdata.2017.122, 2017.

Kattge, J., Bönisch, G., Díaz, S., Lavorel, S., Prentice, I. C., Leadley, P., Tautenhahn, S., Werner, G. D. A., Aakala, T., Abedi, M., Acosta, A. T. R., Adamidis, G. C., Adamson, K., Aiba, M., Albert, C. H., Alcántara, J. M., Alcázar C, C., Aleixo, I., Ali, H., Amiaud, B., Ammer, C., Amoroso, M. M., Anand, M., Anderson, C., Anten, N., Antos, J., Apgaua, D. M. G., Ashman, T., Asmara, D. H., Asner, G. P., Aspinwall, M., Atkin, O., Aubin, I., Baastrup-Spohr, L., Bahalkeh, K., Bahn, M., Baker, T., Baker, W. J., Bakker, J. P., Baldocchi, D., Baltzer, J., Banerjee, A., Baranger, A., Barlow, J., Barneche, D. R., Baruch, Z., Bastianelli, D., Battles, J., Bauerle, W., Bauters, M., Bazzato, E., Beckmann, M., Beeckman, H., Beierkuhnlein, C., Bekker, R., Belfry, G., Belluau, M., Beloiu, M., Benavides, R., Benomar, L., Berdugo-Lattke, M. L., Berenguer, E., Bergamin, R., Bergmann, J., Bergmann Carlucci, M., Berner, L., Bernhardt-Römermann, M., Bigler, C., Bjorkman, A. D., Blackman, C., Blanco, C., Blonder, B., Blumenthal, D., Bocanegra-González, K. T., Boeckx, P., Bohlman, S., Böhning-Gaese, K., Boisvert-Marsh, L., Bond, W., Bond-Lamberty, B., Boom, A., Boonman, C. C. F., Bordin, K., Boughton, E. H., Boukili, V., Bowman, D. M. J. S., Bravo, S., Brendel, M. R., Broadley, M. R., Brown, K. A., Bruelheide, H., Brumnich, F., Bruun, H. H., Bruy, D., Buchanan, S. W., Bucher, S. F., Buchmann, N., Buitenwerf, R., Bunker, D. E., et al.: TRY plant trait database – enhanced coverage and open access, Global Change Biology, 26, 119–188, https://doi.org/10.1111/gcb.14904, 2020.

Kern, S.: MODIS Collection 6.1 Sinusoidal Tiles Yearly gap-filled Gross and Net Primary Production (Version 2024_fv0.01), https://doi.org/10.25592/uhhfdm.14633, 2024.

Kikuzawa, K., Onoda, Y., Wright, I. J., and Reich, P. B.: Mechanisms underlying global temperature-related patterns in leaf longevity: Mechanism of leaf longevity patterns, Global Ecology and Biogeography, 22, 982–993, https://doi.org/10.1111/geb.12042, 2013.

https://doi.org/10.5194/egusphere-2025-6002
Preprint. Discussion started: 17 December 2025

King, D. A.: The Adaptive Significance of Tree Height, The American Naturalist, 135, 809–828, https://doi.org/10.1086/285075, 1990.

Korasidis, V. A., Wing, S. L., Shields, C. A., and Kiehl, J. T.: Global Changes in Terrestrial Vegetation and Continental Climate During the Paleocene-Eocene Thermal Maximum, Paleoceanog and Paleoclimatol, 37, e2021PA004325, https://doi.org/10.1029/2021PA004325, 2022.

Kreft, H. and Jetz, W.: Global patterns and determinants of vascular plant diversity, Proc. Natl. Acad. Sci. U.S.A., 104, 5925–5930, https://doi.org/10.1073/pnas.0608361104, 2007.

Kristensen, T. N., Ketola, T., and Kronholm, I.: Adaptation to environmental stress at different timescales, Annals of the New York Academy of Sciences, 1476, 5–22, https://doi.org/10.1111/nyas.13974, 2020.

Lang, N., Jetz, W., Schindler, K., and Wegner, J. D.: A high-resolution canopy height model of the Earth, Nat Ecol Evol, 7, 1778–1789, https://doi.org/10.1038/s41559-023-02206-6, 2023.

Liu, H., Ye, Q., and Wiens, J. J.: Climatic-niche evolution follows similar rules in plants and animals, Nat Ecol Evol, 4, 753–763, https://doi.org/10.1038/s41559-020-1158-x, 2020.

Liu, J., Ryu, Y., Luo, X., Dechant, B., Stocker, B. D., Keenan, T. F., Gentine, P., Li, X., Li, B., Harrison, S. P., and Prentice, I. C.: Evidence for widespread thermal acclimation of canopy photosynthesis, Nat. Plants, 10, 1919–1927, https://doi.org/10.1038/s41477-024-01846-1, 2024.

Lloyd, J. and Taylor, J. A.: On the temperature dependence of soil respiration, Functional Ecology, 8, 315–323, https://doi.org/10.2307/2389824, 1994.

Martínez-Meyer, E. and Peterson, A. T.: Conservatism of ecological niche characteristics in North American plant species over the Pleistocene-to-Recent transition, Journal of Biogeography, 33, 1779–1789, https://doi.org/10.1111/j.1365-2699.2006.01482_33_10.x, 2006.

Matthaeus, W. J., Macarewich, S. I., Richey, J., Montañez, I. P., McElwain, J. C., White, J. D., Wilson, J. P., and Poulsen, C. J.: A Systems Approach to Understanding How Plants Transformed Earth's Environment in Deep Time, Annu. Rev. Earth Planet. Sci., 51, 551–580, https://doi.org/10.1146/annurev-earth-080222-082017, 2023.

McElwain, J. C. and Punyasena, S. W.: Mass extinction events and the plant fossil record, Trends in Ecology & Evolution, 22, 548–557, https://doi.org/10.1016/j.tree.2007.09.003, 2007.

McElwain, J. C., Popa, M. E., Hesselbo, S. P., Haworth, M., and Surlyk, F.: Macroecological responses of terrestrial vegetation to climatic and atmospheric change across the Triassic/Jurassic boundary in East Greenland, Paleobiology, 33, 547–573, https://doi.org/10.1666/06026.1, 2007.

McElwain, J. C., Matthaeus, W. J., Barbosa, C., Chondrogiannis, C., O' Dea, K., Jackson, B., Knetge, A. B., Kwasniewska, K., Nair, R., White, J. D., Wilson, J. P., Montañez, I. P., Buckley, Y. M., Belcher, C. M., and Nogué, S.: Functional traits of fossil plants, New Phytologist, 242, 392–423, https://doi.org/10.1111/nph.19622, 2024.

Mejía-de-Dios, J.-A. and Mezura-Montes, E.: Metaheuristics: A Julia Package for Single- andMulti-Objective Optimization, JOSS, 7, 4723, https://doi.org/10.21105/joss.04723, 2022.

https://doi.org/10.5194/egusphere-2025-6002
Preprint. Discussion started: 17 December 2025

Miralles, D. G., Holmes, T. R. H., De Jeu, R. A. M., Gash, J. H., Meesters, A. G. C. A., and Dolman, A. J.: Global land-surface evaporation estimated from satellite-based observations, Hydrol. Earth Syst. Sci., 15, 453–469, https://doi.org/10.5194/hess-15-453-2011, 2011.

Monteith, J. L.: Accommodation between transpiring vegetation and the convective boundary layer, Journal of Hydrology, 166, 251–263, https://doi.org/10.1016/0022-1694(94)05086-D, 1995.

Payne, J. L., Lehrmann, D. J., Wei, J., Orchard, M. J., Schrag, D. P., and Knoll, A. H.: Large Perturbations of the Carbon Cycle During Recovery from the End-Permian Extinction, Science, 305, 506–509, https://doi.org/10.1126/science.1097023, 2004.

Pugh, T. A. M., Rademacher, T., Shafer, S. L., Steinkamp, J., Barichivich, J., Beckage, B., Haverd, V., Harper, A., Heinke, J., Nishina, K., Rammig, A., Sato, H., Arneth, A., Hantson, S., Hickler, T., Kautz, M., Quesada, B., Smith, B., and Thonicke, K.: Understanding the uncertainty in global forest carbon turnover, Biogeosciences, 17, 3961–3989, https://doi.org/10.5194/bg-17-3961-2020, 2020.

Reich, P. B., Rich, R. L., Lu, X., Wang, Y.-P., and Oleksyn, J.: Biogeographic variation in evergreen conifer needle longevity and impacts on boreal forest carbon cycle projections, Proceedings of the National Academy of Sciences, 111, 13703–13708, 2014.

Reich, P. B., Sendall, K. M., Stefanski, A., Wei, X., Rich, R. L., and Montgomery, R. A.: Boreal and temperate trees show strong acclimation of respiration to warming, Nature, 531, 633–636, https://doi.org/10.1038/nature17142, 2016.

Retallack, G. J., Veevers, J. J., and Morante, R.: Global coal gap between Permian–Triassic extinction and Middle Triassic recovery of peat-forming plants, Geological Society of America Bulletin, 108, 195–207, https://doi.org/10.1130/0016-7606(1996)108%253C0195:GCGBPT%253E2.3.CO;2, 1999.

Rogger, J.: TREED (v1.0) vegetation model code and input, Zenodo, https://doi.org/10.5281/zenodo.17777279, 2025.

Rogger, J., Judd, E. J., Mills, B. J. W., Goddéris, Y., Gerya, T. V., and Pellissier, L.: Biogeographic climate sensitivity controls Earth system response to large igneous province carbon degassing, Science, 385, 661–666, https://doi.org/10.1126/science.adn3450, 2024.

Rogger, J., Korasidis, V. A., Bowen, G. J., Shields, C. A., Gerya, T. V., and Pellissier, L.: Loss of vegetation functions during the Paleocene–Eocene Thermal Maximum, Nat Commun, https://doi.org/10.1038/s41467-025-66390-8, 2025.

Rüger, N., Condit, R., Dent, D. H., DeWalt, S. J., Hubbell, S. P., Lichstein, J. W., Lopez, O. R., Wirth, C., and Farrior, C. E.: Demographic trade-offs predict tropical forest dynamics, Science, 368, 165–168, https://doi.org/10.1126/science.aaz479, 2020.

Santoro, M., Cartus, O., Carvalhais, N., Rozendaal, D. M. A., Avitabile, V., Araza, A., de Bruin, S., Herold, M., Quegan, S., Rodríguez-Veiga, P., Balzter, H., Carreiras, J., Schepaschenko, D., Korets, M., Shimada, M., Itoh, T., Martínez, Á. M., Cavlovic, J., Gatti, R. C., Liang, J., Lindsell, J., Mitchard, E. T. A., Morel, A., Pascagaza, A. M. P., Ryan, C. M., Slik, F., Laurin, G. V., Verbeeck, H., Wijaya, A., and Willcock, S.: The global forest above-ground biomass pool for 2010 estimated from high-resolution satellite observations, 2010.

https://doi.org/10.5194/egusphere-2025-6002
Preprint. Discussion started: 17 December 2025

Schaphoff, S., von Bloh, W., Rammig, A., Thonicke, K., Biemans, H., Forkel, M., Gerten, D., Heinke, J., Jägermeyr, J., Knauer, J., Langerwisch, F., Lucht, W., Müller, C., Rolinski, S., and Waha, K.: LPJmL4 – a dynamic global vegetation model with managed land – Part 1: Model description, Geosci. Model Dev., 11, 1343–1375, https://doi.org/10.5194/gmd-11-1343-2018, 2018.

Schneider, P. D., Gessler, A., and Stocker, B. D.: Global Photosynthesis Acclimates to Rising Temperatures Through Predictable Changes in Photosynthetic Capacities, Enzyme Kinetics, and Stomatal Sensitivity, J Adv Model Earth Syst, 17, e2024MS004789, https://doi.org/10.1029/2024MS004789, 2025.

Schymanski, S. J., Sivapalan, M., Roderick, M. L., Hutley, L. B., and Beringer, J.: An optimality-based model of the dynamic feedbacks between natural vegetation and the water balance, Water Resources Research, 45, 2008WR006841, https://doi.org/10.1029/2008WR006841, 2009.

Shinozaki, K., Yoda, K., Hozumi, K., and Kira, T.: A quantitative analysis of plant form - the pipe model theory: I. Basic analyses, Japanese Journal of Ecology, 14, 97–105, https://doi.org/10.18960/seitai.14.3_97, 1964.

Sitch, S., Smith, B., Prentice, I. C., Arneth, A., Bondeau, A., and Cramer, W.: Evaluation of ecosystem dynamics, plant geography and terrestrial carbon cycling in the LPJ dynamic global vegetation model, Global Change Biology, 25, 2003.

Sitch, S., Huntingford, C., Gedney, N., Levy, P. E., Lomas, M., Piao, S. L., Betts, R., Ciais, P., Cox, P., Friedlingstein, P., Jones, C. D., Prentice, I. C., and Woodward, F. I.: Evaluation of the terrestrial carbon cycle, future plant geography and climate-carbon cycle feedbacks using five Dynamic Global Vegetation Models (DGVMs), Global Change Biology, 14, 2015–2039, https://doi.org/10.1111/j.1365-2486.2008.01626.x, 2008.

Soh, W. K., Wright, I. J., Bacon, K. L., Lenz, T. I., Steinthorsdottir, M., Parnell, A. C., and McElwain, J. C.: Palaeo leaf economics reveal a shift in ecosystem function associated with the end-Triassic mass extinction event, Nature Plants, 3, 17104, https://doi.org/10.1038/nplants.2017.104, 2017.

Stein, A., Gerstner, K., and Kreft, H.: Environmental heterogeneity as a universal driver of species richness across taxa, biomes and spatial scales, Ecology Letters, 17, 866–880, https://doi.org/10.1111/ele.12277, 2014.

Stemkovski, M., Bernhardt, J. R., Blonder, B. W., Bradford, J. B., Clark-Wolf, K., Dee, L. E., Evans, M. E. K., Iglesias, V., Johnson, L. C., Lynch, A. J., Malone, S. L., Osborne, B. B., Pastore, M. A., Paterson, M., Pinsky, M. L., Rollinson, C. R., Selmoni, O., Venkiteswaran, J. J., Walker, A. P., Ward, N. K., Williams, J. W., Zarakas, C. M., and Adler, P. B.: Ecological acclimation: A framework to integrate fast and slow responses to climate change, Functional Ecology, 39, 1923–1939, https://doi.org/10.1111/1365-2435.70079, 2025.

Stocker, B. D., Wang, H., Smith, N. G., Harrison, S. P., Keenan, T. F., Sandoval, D., Davis, T., and Prentice, I. C.: P-model v1.0: an optimality-based light use efficiency model for simulating ecosystem gross primary production, Geosci. Model Dev., 13, 1545–1581, https://doi.org/10.5194/gmd-13-1545-2020, 2020.

Valentine, H. T. and Mäkelä, A.: Modeling forest stand dynamics from optimal balances of carbon and nitrogen, New Phytologist, 194, 961–971, https://doi.org/10.1111/j.1469-8137.2012.04123.x, 2012.

https://doi.org/10.5194/egusphere-2025-6002
Preprint. Discussion started: 17 December 2025

Wang, H., Atkin, O. K., Keenan, T. F., Smith, N. G., Wright, I. J., Bloomfield, K. J., Kattge, J., Reich, P. B., and Prentice, I. C.: Acclimation of leaf respiration consistent with optimal photosynthetic capacity, Global Change Biology, 26, 2573–2583, https://doi.org/10.1111/gcb.14980, 2020.

Wang, H., Prentice, I. C., Wright, I. J., Warton, D. I., Qiao, S., Xu, X., Zhou, J., Kikuzawa, K., and Stenseth, N. Chr.: Leaf economics fundamentals explained by optimality principles, Sci. Adv., 9, eadd5667, https://doi.org/10.1126/sciadv.add5667, 2023.

Waring, R., Schroeder, P., and Oren, R.: Application of pipe model theory to predict canopy leaf area, Canadian Journal of Forest Research, 12, 556–560, https://doi.org/10.1139/x82-086, 1982.

White, J. D., Montañez, I. P., Wilson, J. P., Poulsen, C. J., McElwain, J. C., DiMichele, W. A., Hren, M. T., Macarewich, S., Richey, J. D., and Matthaeus, W. J.: A process-based ecosystem model (Paleo-BGC) to simulate the dynamic response of Late Carboniferous plants to elevated O_2 and aridification, Am J Sci, 320, 547–598, https://doi.org/10.2475/09.2020.01, 2020.

Wilson, J. P., Montañez, I. P., White, J. D., DiMichele, W. A., McElwain, J. C., Poulsen, C. J., and Hren, M. T.: Dynamic Carboniferous tropical forests: new views of plant function and potential for physiological forcing of climate, New Phytologist, 215, 1333–1353, https://doi.org/10.1111/nph.14700, 2017.

Wing, S. L. and Currano, E. D.: Plant response to a global greenhouse event 56 million years ago, American J of Botany, 100, 1234–1254, https://doi.org/10.3732/ajb.1200554, 2013.

Wing, S. L., Harrington, G. J., Smith, F. A., Bloch, J. I., Boyer, D. M., and Freeman, K. H.: Transient Floral Change and Rapid Global Warming at the Paleocene-Eocene Boundary, Science, 310, 993–996, https://doi.org/10.1126/science.1116913, 2005.

Wright, I. J., Reich, P. B., Westoby, M., Ackerly, D. D., Baruch, Z., Bongers, F., Cavender-Bares, J., Chapin, T., Cornelissen, J. H. C., Diemer, M., Flexas, J., Garnier, E., Groom, P. K., Gulias, J., Hikosaka, K., Lamont, B. B., Lee, T., Lee, W., Lusk, C., Midgley, J. J., Navas, M.-L., Niinemets, Ü., Oleksyn, J., Osada, N., Poorter, H., Poot, P., Prior, L., Pyankov, V. I., Roumet, C., Thomas, S. C., Tjoelker, M. G., Veneklaas, E. J., and Villar, R.: The worldwide leaf economics spectrum, Nature, 428, 821–827, https://doi.org/10.1038/nature02403, 2004.

Xu, Z., Hilton, J., Yu, J., Wignall, P. B., Yin, H., Xue, Q., Ran, W., Li, H., Shen, J., and Meng, F.: End Permian to Middle Triassic plant species richness and abundance patterns in South China: Coevolution of plants and the environment through the Permian–Triassic transition, Earth-Science Reviews, 232, 104136, https://doi.org/10.1016/j.earscirev.2022.104136, 2022.

Xu, Z., Yu, J., Yin, H., Merdith, A. S., Hilton, J., Allen, B. J., Gurung, K., Wignall, P. B., Dunhill, A. M., Shen, J., Schwartzman, D., Goddéris, Y., Donnadieu, Y., Wang, Y., Zhang, Y., Poulton, S. W., and Mills, B. J. W.: Early Triassic super-greenhouse climate driven by vegetation collapse, Nat Commun, 16, 5400, https://doi.org/10.1038/s41467-025-60396-y, 2025.

https://doi.org/10.5194/egusphere-2025-6002
Preprint. Discussion started: 17 December 2025

Zhang, L., Hu, Z., Fan, J., Zhou, D., and Tang, F.: A meta-analysis of the canopy light extinction coefficient in terrestrial ecosystems, Front. Earth Sci., 8, 599–609, https://doi.org/10.1007/s11707-014-0446-7, 2014.

Zhu, L., Bloomfield, K. J., Asao, S., Tjoelker, M. G., Egerton, J. J. G., Hayes, L., Weerasinghe, L. K., Creek, D., Griffin, K. L., Hurry, V., Liddell, M., Meir, P., Turnbull, M. H., and Atkin, O. K.: Acclimation of leaf respiration temperature responses across thermally contrasting biomes, New Phytologist, 229, 1312–1325, https://doi.org/10.1111/nph.16929, 2021.